Spring 2016

Preliminary Investigation of Commercially Available Pluronics as UV Curable 3D Printing Inks for Tissue Engineering Applications

A'Lester Cordell Allen
San Jose State University

Recommended Citation

Allen, A'Lester Cordell, "Preliminary Investigation of Commercially Available Pluronics as UV Curable 3D Printing Inks for Tissue Engineering Applications" (2016). *Master's Theses*. 4677.
DOI: https://doi.org/10.31979/etd.r2z2-q6cz
https://scholarworks.sjsu.edu/etd_theses/4677

PRELIMINARY INVESTIGATION OF COMMERCIALLY AVAILABLE PLURONICS AS UV CURABLE 3D PRINTING INKS FOR TISSUE ENGINEERING APPLICATIONS

A Thesis

Presented to

The Faculty of the Department of Biomedical, Chemical, and Materials Engineering

San José State University

In Partial Fulfillment

of the Requirements for the Degree

Master of Science

By

A'Lester Cordell Allen

May 2016

The Designated Thesis Committee Approves the Thesis Titled

PRELIMINARY INVESTIGATION OF COMMERCIALLY AVAILABLE PLURONICS AS UV CURABLE 3D PRINTING INKS FOR TISSUE ENGINEERING APPLICATIONS

by

A'Lester Cordell Allen

APPROVED FOR THE DEPARTMENT OF BIOMEDICAL, CHEMICAL, AND MATERIALS ENGINEERING

SAN JOSÉ STATE UNIVERSITY

May 2016

Dr. Folarin Erogbogbo	Department of Biomedical, Chemical, and Materials Engineering
Dr. Brooke Lustig	Department of Chemistry
Dr. Amanda Engler	IBM Almaden Research Center

ABSTRACT

PRELIMINARY INVESTIGATION OF COMMERCIALLY AVAILABLE PLURONICS AS UV CURABLE 3D PRINTING INKS FOR TISSUE ENGINEERING APPLICATIONS

by A'Lester Cordell Allen

Three-dimensional printing (3DP) emerged from simple beginnings in the field of additive manufacturing (AM) over 31 years ago as an economical technique for rapid prototyping. Now 3DP has become the premier method for fabricating materials from unique consumer products to lifesaving customized human organs. Current challenges in bioprinting center around balancing material properties such as stiffness, yield strength, and surface chemistry with non-Newtonian fluid flow to construct interconnected, porous scaffolding geometries that simulate the complex vasculature found in the extracellular matrix (ECM) of the human body needed to promote cell growth and regeneration. In this study, several copolymers of poly(ethlyene oxide) and poly(propylene oxide) with a triblock structure were characterized using oscillatory shear measurements and thermogravimetric instruments to investigate the relationship between storage and loss moduli (G' and G") and printing behavior. The relationship between complex viscosity (η^*), yield stress (τ_y), and fluid flow through a syringe yields some indirect correlations that depend on testing procedure. The overall relationship was more complex than originally understood. In the end, several self-supporting complex geometries were successfully printed using a photocurable formulations waxy (Pluronic P85, Jeffamine ED 2003) and liquid (Pluronic L121) triblock copolymers.

ACKNOWLEDGEMENTS

This project was one of the biggest challenges and richest parts of my career as a researcher thus far. I am truly grateful to the many people who have helped me to succeed, pushed me to grow professionally, and exposed me to new areas of research. I would like to thank some people without whom this experience would not have been possible.

First, I am deeply appreciative to Dr. Melanie McNeil for connecting me to IBM Almaden. Next, I am indebted to both of my research mentors, Dr. Amanda Engler and Dr. Folarin Erogbogbo. Amanda, you have given me a better sense of how to tackle complex problems that will help me for the rest of my life. You were also a friend, a big sister, and a motivator. I will always be grateful for your mentorship.. Dr. E., thank you for taking me in as one of your students,validating my skills, and instilling within me a sense of self-reliance. Next, I would also like to thank Dr. Brooke Lustig for helping me to refine my design of experiments and documentation and writing skills. Additionally, I am thankful to Cynthia Farmer, Dr. Al Nelson, Dr. Hareem Maune, Dr. Rudy Worjtecki, Dr. Wei Han, Dr. Jane Frommer, Leslie Krupp, Erik Lara, Teddie Magbitang, and Andy Tek for the countless times that I received help from the adept and kind people at IBM Almaden. Thank you Neil Peters for enabling me to complete parts of my project at SJSU, and Elliot Baker, Henry Vo, and Ngoc Huynh at SJSU for collaborating with me.

Lastly, I dedicate this thesis to my beloved family. I thank my father, Henry Allen, who has always believed in me, my husband, Jeffrey Chern Jr., who has given me so much emotional support as well as practical editing tools. Thank you for also being

patient with me despite so many long nights and cancelled trips. I would also like to thank my sister, Jessica Allen, for being my rock and sounding board.

Because of this experience and the support from many faculty members and staff at San Jose State University, research staff and contractors at IBM Almaden Research Center, and my family I will leave this experience and San Jose State University a more confident, knowledgeable and prepared individual. I will apply all that I have learned in my studies as a chemistry doctoral student at the University of California, Santa Cruz.

TABLE OF CONTENTS

LIST OF FIGURES

LIST OF TABLES

CHAPTER ONE
INTRODUCTION

The two fields of additive manufacturing (AM) and tissue engineering (TE) are heavily dependent upon the materials used. The field of AM was founded on using synthetic polymers to construct models. Within the last decade, printing technology has been applied to TE which creates a need for more biocompatible materials. Simultaneously, TE is facing a need for diversified materials that can be tailored to the specific needs of different tissue types. Currently hydrogel materials have been used with limited success in growing organs. This is due in part to suboptimal materials selection and to the limitations of printing technology.

Although a perfect fit has not been found, AM continues to revolutionize the field of TE with regenerative treatments that not only can be mass produced, but also easily customized. Bioprinting has been limited by the inability to comprehensively recreate the environment of human tissue. The work presented here will give an in-depth look into the problems and previous research needed to establish a foundation to help advance this interdisciplinary field.

1.1 Tissue Engineering

The rapidly developing field of TE continually advances modern medicine. Bone and vascular tissues are the current focus of research. Over 2.2 million bone-grafting procedures occur annually at cost of 28 million dollars [1-4]. The field of TE has the potential to replicate all tissues of the human body to grow organs and other complex structures. Due to the growth of our aging population, TE is expected to continually develop and become a vital technology for aiding patients waiting for an organ transplant.

The idea of using one tissue to replace another is not new. The essence of TE is the regeneration of our broken bodies to further improve the frailty of the human existence. As early as the sixteenth century, Tagliacozzi of Bologna, Italy, reported constructing a nose replacement from forearm skin. His research marked the beginning of new fields of medicine and most recently, engineering. The field has progressed to be globally recognized with a Nobel Prize in Physiology or Medicine for the discovery that mature cells can be reprogrammed to give rise to different cell types [5]. Another advantage of TE is that long term success of many structures is due to 3D scaffolding. Research in TE brings potency to reconstructive surgery, revolutionizes tissue grafting, and brings much needed attention to bioengineering.

1.2 Three Dimensional Printing Applied To Tissue Engineering

Modern advances in AM, specifically rapid prototyping and versatile printing methods, have revolutionized the field of TE. Rapid prototyping allows for quick manufacture of specialized geometries. The focal printing method of this paper is direct ink writing (DIW) which grew out of ink jet and three dimensional printing (3DP) technologies. A DIW system is characterized by a computer-controlled system that moves the translation stage or the ink deposition device along the Cartesian coordinate system nozzle to quickly and cheaply fabricate 3D architectures via layer-by-layer deposition [6]. This method gives more precision than George Whiteside's foundational work of printing human organ cells on a microchip [7]. Although DIW includes micro-pen writing, fused deposition, droplet-based deposition, and hot melt printing, the approach discussed here is a filamentary-based method using a pressurized system to deposit the ink and is known as robotic deposition [8]. The Lewis group at Harvard University prominently utilizes DIW to construct 3D periodic structures used for both TE and electronic applications [1, 9-12]. The DIW printing method is ideal for printing tissues because it operates without complicated external masks, bulk liquid solutions, and under ambient conditions.

1.3 Scaffolding Materials for Three Dimensional Printing

Hydrogel scaffolds are used because they most closely replicate the environment of human cells. Material selection for hydrogels hinges upon biocompatibility, low toxicity, and mechanical properties. Cell death currently limits the widespread application of TE to larger organ transplants especially when incorporating human cells into the extracellular matrix. Cell survival also depends on creating interconnected networks to promote the repair and regenerate tissues [13]. Hydrogels can absorb a large content of cell nutrients. The design of the scaffold balances material properties, e.g. stiffness, strength, and surface chemistry. Current popular materials such as Pluronic F-127 lack the physical strength necessary to construct self-supporting structures. Typically soft hydrogels gain strength from adding a UV curable crosslinking network by fictionalization with acrylates [14]. Polymer ink design for TE scaffolding depends primarily on characterization by rheology and screening for biocompatibility [6, 15]. Rheology shears the material to determine the viscosity, loss and storage moduli, and gel time [16].

1.4 Significance

There are many applications of 3D printed tissue scaffolds. Of primary importance is helping the increasing number of aging members of the population. Secondary uses are to improve the field of orthopedics with healing bone fractures, tumor resections, and osteoporosis. Finally, the work of improving bioprinting directly affects organ transplant patients. In the US alone, there are 100,000 people, on average, on the waiting list for kidneys, livers, hearts, and new lungs. Many patients die from organ failure while waiting. In addition to fundamental research on cell growth and migration, tissue scaffolding affects the human population and offers a potential solution to many health care problems.

1.5 Conclusion

The development of novel 3D printing inks for TE depends on engineering the materials that are capable of retaining their shape after extrusion. The materials must also be biocompatible and have the porosity and interconnected networks necessary to transport nutrients to growing cells. Work from the Lewis Group at Harvard has laid the foundation for scaffolding of hydrogels. The work from several other research groups from Bioengineering departments at Rice University, Virginia Tech, and Stanford University has also laid the foundation for characterizing the material properties of polymers for scaffolding soft and hard tissue. The work presented in this thesis will capitalize on their work to develop a stronger alternative to hydrogels ECM scaffolds.

CHAPTER TWO
LITERATURE REVIEW

Although AM emerged in the late twentieth century, only recently has bioprinting become a strong field that promises printing of organs and microvascular networks using ink jet technology. The unique application of DIW printing to TE enables inexpensive, quick scaffold development. The two areas of 3D printing that use curable polymers are stereolithography (SL) and direct write printing. There is a current need for stronger materials that are self-supporting. The next several chapters will focus on materials currently used in TE and methods to improve their strength. This literature review will contrast different biocompatible materials, printing techniques, and strengthening mechanisms.

2.1 Characterization of Non-Newtonian Liquids

Non-Newtonian fluids make up the vast majority of materials used in bioprinting. The science of characterizing non-Newtonian fluids is called rheometry. Rheometry measures not only viscosity but also the normal stresses and the materials’ viscoelastic response. Rheology is the study of the viscoelastic properties of polymeric materials. Rheological characterization is crucial for quantifying the shear modulus, gel point, and viscosity that informs a material's thixotropic and printing behavior. Foundational work by the Lewis group was used to establish a baseline target for the properties of hydrogels and waxy printing materials [8, 17]. The accuracy of rheology depends on shearing the material within its linear viscoelastic regime (LVR). Three tests must be done in order to establish the bounds of the LVR [16]. Many researchers skip these tests, making their results hard to reproduce. Rheology is a large field that studies polymeric in a variety of industries including plastics industry, food industry, and printing industry. An example of the parallel plate geometry can be seen in Figure 1. The upper plate oscillates at an angular frequency, applying shear stress (τ) to the material [2].

$$\eta^{*} = \eta^{\prime} + i\eta^{\prime\prime}$$

Equation 1

Equation 1 defines the viscoelastic response for Non-Newtonian polymer melts. In Equation 1, η^{*} is the complex viscosity which is composed of real and imaginary parts, $\eta^{\prime}$ and η'', respectively. Complex viscosity is models the frequency dependence of viscosity during forced harmonic oscillation as found in parallel plate rheology. The terms $\eta^{\prime}\ and\ \eta^{\prime}{}'$ contain two terms which compose the dynamic modulus, the storage and loss moduli.

$$\eta' = \frac{G^{\prime}{}'}{\omega} \qquad \text{Equation 2}$$

$$\eta^{\prime}{}' = \frac{G^{\prime}}{\omega} \qquad \text{Equation 3}$$

Equations 2 and 3 relate the real and imaginary parts to the loss and storage moduli G’’ and G’. Eta double prime (η'') is the in-phase response to τ which is used to calculate G’. The storage modulus is a measure of the stiffness or solid-like behavior of the material, and for a viscoelastic material, a higher G’ correlates to a hard material under the test conditions [16]. Viscosity of the material and the change in velocity of the shearing plates describe the mechanical operations of shear force. Eta prime (η') is the out of phase response that measures the liquid-like behavior of the polymeric material that is used to find the G”. Omega (ω) is the angular frequency, $\dot{\gamma}$ is the shear rate, and t is the time [18]. The shear rate is a controllable parameter that is held constant for these reactions. G’, G”, and ŋ are all rheological parameters which provide a quantitative basis for comparing the mechanical properties of each polymer.

$$\tau^{app}{}_{y} = \tau(0.1\, G_0{}^{'}) \qquad \text{Equation 4}$$

Equation 4, where $\tau^{app}{}_{y}$ is the applied shear stress, τ is the shear stress, and $G_0{}^{'}$ is the storage modulus at the plateau.

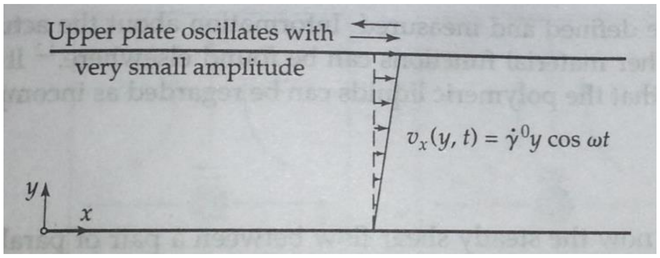

Figure 1. Small-amplitude oscillatory motion for a highly viscous material using parallel plates [2] (reprinted with permission from John Wiley and Sons).

Furthermore, the complex viscosity that was shown in Equation 1 relates to the other measurements of viscosity through an empirical relationship called the Cox-Merz Rule. There is an empirical relationship between steady state viscosity found using shear rate and complex viscosity found using oscillatory shear measurements. Equation 5 displays an empirical relationship called the Cox-Merz Equation.

$$|\eta(\dot{\gamma})|_{\dot{\gamma}=\omega} = |\eta^{*}(\omega)| \qquad \text{Equation 5}$$

Equation 5, where $\eta(\dot{\gamma})$is the apparent viscosity as a function of strain rate, $\dot{\gamma}$ is the strain rate, ω is the angular frequency, and $\eta^{*}(\omega)$, is the complex viscosity as a function of angular frequency.

The desired result of an oscillatory shear stress test is the determination of the shear thinning behavior of a material, G', and the shear yield stress (τ_y) which is a measure of the stress at which the material begins to flow. As seen in Figure 2a, the shear thinning behavior is found via a steady-state oscillatory test that calculates the apparent viscosity as a function of the shear strain rate. A linear decreasing slope is characteristic of shear thinning materials while a flat slope is characteristic of Newtonian fluids which have a constant viscosity. Figure 2b shows the results of a dynamic oscillatory shear stress test where sample G’ and G’’ are shown for harder viscoelastic materials (in blue) and softer viscoelastic materials (in red). For Figure 2b, the G' plateau is the flat linear portion, and τ_y occurs within the yielding zone around the drop.

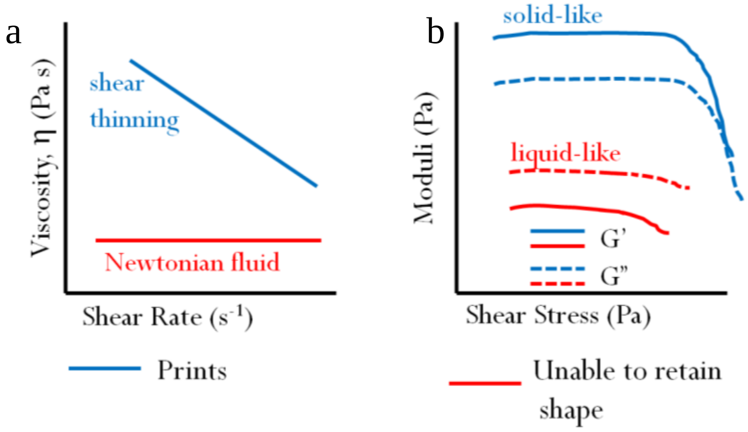

Figure 2. Typical curve from a) steady state and b) dynamic oscillatory shear tests.

There are several discrepancies in literature for determining both G' and τ_y. The differences arise for several reasons. Both properties are dependent upon several testing conditions such as temperature, pressure, time, and strain rate similar to Newton's definition of viscosity as seen in Equation 6.

$$\eta(T, p, t, \gamma) = \frac{\tau}{\dot{\gamma}} \qquad \text{Equation 6}$$

Equation 6, where η is the apparent viscosity, T is temperature, p is pressure, t is time, γ is shear strain, τ is the shear stress, and $\dot{\gamma}$ is the strain rate.

The absolute values for τ_y are also difficult to determine because yielding occurs over a range of values. The overwhelming prevalent method for determining G' is to quote the value for the stable plateau. The Lewis group consistently states the value for G' in Pa at a shear stress of 10 Pa. Equation 4 references one method mentioned by Zukoski et al. to find the applied shear stress based on the 90 percent drop in G' from the initial plateau [19]. Figures 3a and b show another method based on the observation by Houwink in 1958 that show two yield stresses. This can be thought of as a yield stress zone where the upper yield stress is the beginning of the yield zone and marks the transition from solid-like to fluid-like behavior. The lower yield stress marks the final transition, or also known as the gel point, where the fluid-like behavior is dominant and marks the end of the linear plateau [16, 20]. Another model for finding the yield stress as seen in Figure 3 c was more recently developed; G' is converted into a stress called the elastic stress by Khan et al. [21]. This model, which will be called the stress-strain model, then plots the elastic stress as a function of shear strain. The idea is based on the stress strain curves of alloys where the slope is the elastic modulus also known as Young's modulus which is a measure of the materials resistance to plastic deformation. Similarly, in the model developed by Khan et al., the slope of the graph is G', but unlike stress-strain curves for alloys, there is a characteristic peak which is denoted as the yield stress which provides a definitive number. The methods listed above will be used to determine the most accurate value for τ_y.

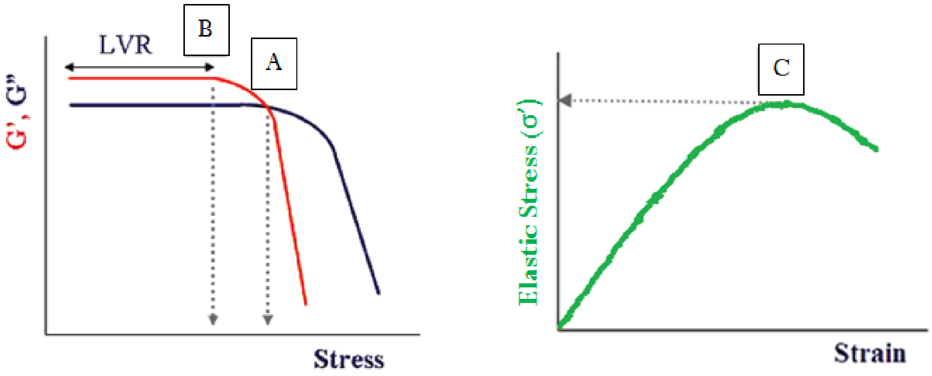

Figure 3. Different methods for determining yield Stress. a) and b) Lower and Upper yield stress limits according to Houwink (1958). c) Stress-Strain curve generated by plotting G'/γ according to Khan (2003).

In addition to rheological characterization, Tensile testing, Dynamic Mechanical Analysis, and Thermal Gravimetric Analysis are typical methods used to test the mechanical strength of polymers. The motive for using DMA is that smaller loads can be applied to the specimens. This is in contrast to tensile testing where the Instron grips are stronger than the tensile strength of the material being measured. The DMA parameters were sinusoidal tensile oscillation with a static force of 0.010 N at a fixed frequency of 1 Hertz to slowly deform the sample. The clamping arrangement is shown in the Figure 4. The measurements were taken as two heating cycles from -20°C to 100°C, at a temperature ramp rate of 5°C per minute to more accurately determine the storage and loss moduli.

Figure 4. Clamping arrangement of the DMA tension measurement showing both sides of the specimen being fixed, but only one side being loaded.

Polymers are viscoelastic materials that have a delayed mechanical response to an applied force. The storage modulus is the in-phase component of the response. This is a measure of stiffness or elastic behavior. Loss modulus is the out-of-phase component. Tan delta is the ratio of the loss modulus to the storage modulus and is often called the damping component.

Thermal gravimetric analysis (TGA) is a technique which measures the change in mass of a material as a function of temperature. For polymers, it is mainly used to investigate chemical behaviors upon heating and cooling. It is also used to characterize kinetics, mechanisms, and processes. Thermal stability of the polymers is often found by TGA. Tensile tester such as an Instron is typically used to generate stress versus strain graphs, and determine the yield stress, elastic modulus, ultimate tensile stress, and percent elongation at fracture of the testing materials.

2.2 Results of Characterization

The two materials commonly used by the Lewis group to print a microvascular network are a Fugitive Organic Wax and Pluronic F127. Organic wax is a 40 wt% mixture of petroleum jelly, specifically trademarked Vaseline, and paraffin [16]. Paraffin is a wax used to make candles. Vaseline is a low molecular weight polymer, while paraffin is a microcrystalline wax that provides structure to the overall mixture. The molecular weights of the starting materials and the mixture can be seen in Table 1. The mixture has a higher molecular weight than Vaseline but a lower molecular weight than paraffin. Under an optical microscope, amorphous regions are dark and crystalline regions are light. The color gradient is used to evaluate homogenous mixing. This mixture of Vaseline and paraffin was chosen because of its similar chemical structure to commercially available Prussian blue paste, which consists of a mixture of paraffin wax, mineral oil, and ferric ferrocyanide nanoparticles.

Table 1. Molecular weights of the components of organic wax and a 40 wt% paraffin wax in Vaseline.

Polymer	Molecular Weight (amu)
Vaseline	840
Paraffin Wax	1450
Organic Wax Ink	1050

Therriault et al. (2007) investigated the G', G", and η^* values for 40 wt% organic wax. In the plateau region, the storage modulus was found to be just under 8.0×10^5 Pa, while the complex viscosity and loss moduli were found to be 7.0×10^4 Pa and 0.5×10^5 Pa, respectively as seen in Figure 5.

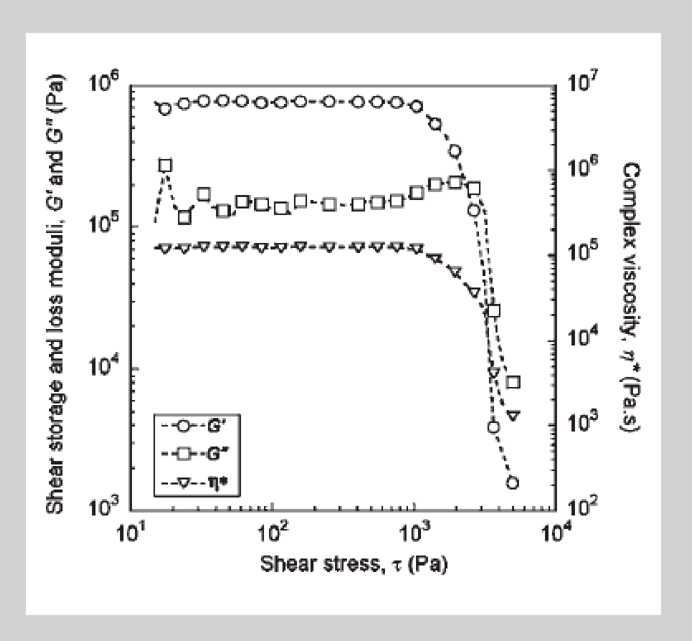

Figure 5. Complex viscosity, elastic, and loss moduli as a function of shear stress for 40wt% organic wax [16] (Reprinted with permission from Applied Rheology).

Neither paraffin nor petroleum jelly is biocompatible, so the Lewis group progressed to materials that could be possible inks such as F127. Pluronic F127, is a triblock copolymer constructed from poly (ethylene oxide) (PEO) and poly (propylene oxide) (PPO) in PEO-PPO-PEO sequence [22]. Poly (ethlyene oxide) is hydrophillic, while poly (propylene oxide) is hydrophobic. This allows a temperature or concentration-controlled gelation. Acrylate end groups are added to make a cross-linked hydrogel forming the structure in Figure 6.

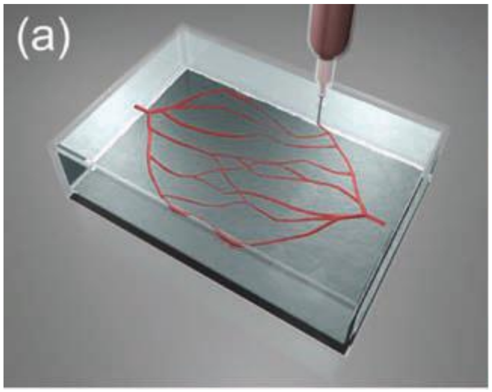

Figure 6. CAD printing of a microvascular network [23] (reprinted with permission from John Wiley and Sons).

There are two important aspects to choosing a 3D printing ink: the material's rigidity and change in viscosity over time. Overall, Newtonian fluids can be characterized by viscosity only. Non-Newtonian fluids, which are far more numerous, are complex. Rheology is a technique that measures the viscoelastic properties of non-Newtonian fluids such the storage modulus (G'), loss modulus (G"), and viscosity (η) of these materials. G' is a measure of the solid-like behavior of a material and is better known by materials engineers as the elastic modulus. The properties of non-Newtonian materials change with respect to shear stress. For example, pressure applied to a bottle of ketchup lowers the viscosity enough for the material to flow through the nozzle, then solidify on a plate. Other examples of shear thinning materials include toothpaste, paint, and polymers. Rheology is capable of measuring these changes with respect to several variables such as time, shear stress, shear rate, and strain. For a material to shear thin, the viscosity decreases as shear stress increases.

Petroleum jelly is very similar to a commercially available ink called Prussian Blue. The mixture of Vaseline and paraffin was continuously heated and stirred to remove any phase differences.

Pluronic F127 was chosen to make an ink for three reasons:.(1) The hydrophillic-hydrophobic interactions allow the material to form flower like micelles; (2) Pluronic F127 is soluble in water, but above the critical micelle concentration (CMC) or the critical micelle temperature (CMT); (3) Pluronic F127 exhibits a phase change and becomes a gel. The hydrogel ink shear thins, allowing extrusion through a needle. These properties allowed a simple optimization to print in the gel matrix to print Figure 7. The storage modulus at 25^{o}C of F127 was found to be $5.0\text{x}10^{4}$ Pa. The diacrylate hydrogels experienced a slight decrease in storage modulus. A summary of the temperature and concentration results of the study can be seen in Table 2. Although it is possible to slightly increase the stiffness of F127 hydrogels, the storage modulus of F127 hydrogels are significantly lower than that of Organic Wax inks.

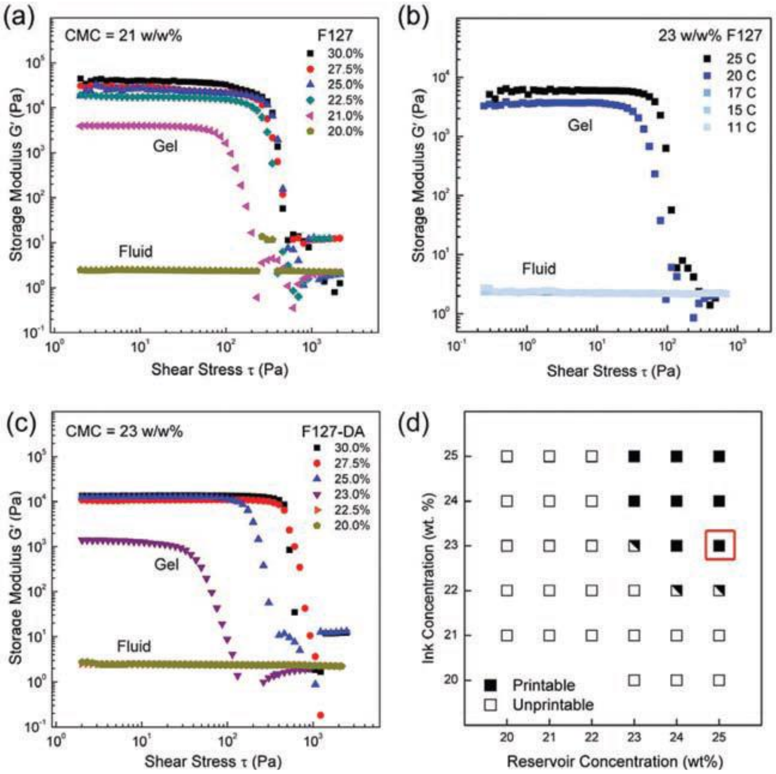

Figure 7. Storage modulus of a) the starting material Pluronic F127, b) the reacted Pluronic F127 DA, and c) the hydrogel ink at 23 wt% [19] (reprinted with permission from John Wiley and Sons).

Table 2. Results of the Lewis group's study of organic wax and F127, and F127DA hydrogels.

Material	Shear Yield Stress (Pa)
23 wt% Pluronic F127 at 20 and 50°C	20-50
21-30 wt%Pluronic F127	90-200
23-30 wt% Pluronic F127 DA	3-300
Organic wax	1000

Rheometric analysis of organic ink samples revealed that G', G" vary with an increasing τ. Using G' and G", the complex viscosity was calculated from combining

Equations 1-3 to derive Equation 7. [16]. Rheological measurements, as seen in Figure 7, revealed the linear viscoelastic region (LVR) which is where the material deforms elastically, i.e., the mechanical properties are independent of the applied stress.

$$\eta^* = \frac{G' + G''}{i\omega} \qquad \text{Equation 7}$$

Equation 7 relates the complex viscosity directly to G', G", and ω.

When the pressure is held constant, the flow rate (Q) depends on the write speed (v) and diameter (D) of the nozzle as seen in Equation 8 [16]. The results were optimized to find the correct parameters to determine the diameter of the channel in the gel matrix to equal the diameter of the gel coming from the nozzle. With channel sizes varying from 18µm to 170 µm (0.5 to 5.5D_{nozzle}), a nozzle size of 30 µm was needed. Overall, the results of these series of rheological experiments were appropriate ratios of Pluronic F127 to Pluronic F127DA, nozzle diameter to channel size, write speed, and volumetric flow rate.

$$Q = 0.25\, D^2{}_{nozzle}\, v \qquad \text{Equation 8}$$

Equation 8, where Q is the flow rate, D is the diameter of the nozzle, and v is the write speed.

The mechanical properties of materials that behave like Newtonian fluids are well understood and follow Newton's law of viscosity. Equation 8 shows a characteristic resistance to flow for each material given shear stress (force per area). For Newtonian fluids, the velocity gradient is linear with movement away from the shear stress. The fluids not described by Equation 7 are structurally complex and include polymers over 5000 amu and are called non-Newtonian fluids. The viscosities of non-Newtonian fluids depend on the velocity gradient. The next sections detail the significance, strengths, and limitations of materials currently used in bioprinting.

2.3 Review of Additive Manufacturing

Additive manufacturing (AM) uses computer-generated designs to provide physical models. Professional fields began to use AM as a method to rapidly produce physical models to better understand often hidden structures. One of the most important aspects of AM is computer-aided design (CAD). In the 1990s, 3D modeling began to develop into a specialized field called rapid prototyping (RP). Rapid prototyping rose to popularity in professional fields such as science, engineering, medical, art, and marketing as a way to analyze structures that only existed as images. Figure 8 displays an overview of the AM process. The process starts with designing the conceptual model, then constructing a CAD model. Next a recursive loop occurs to optimize the system until the results are satisfactory.

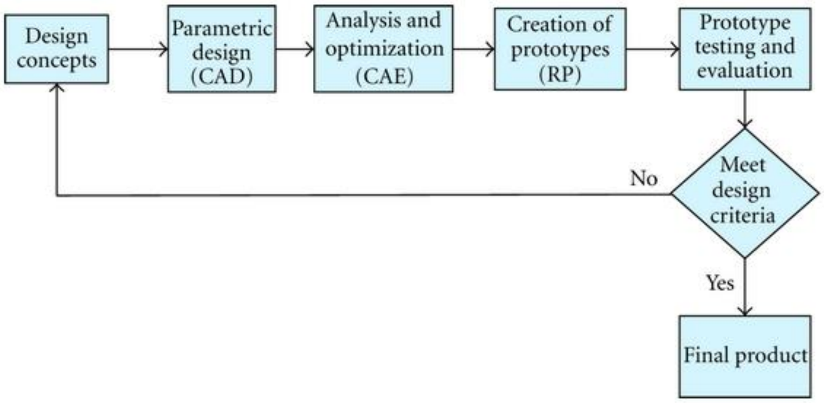

Figure 8. Product development cycle of additive manufacturing [25] (reprinted with permission from Hindawi Publishing Corporation).

There are traditionally three branches in AM, as seen in Figure 9: liquid, solid, and powder based. Polymer processing typically is included in the liquid-based techniques such as extrusion and fused deposition modeling (FDM), inkjet, and stereolithography (SL). Laminated object manufacturing (LOM) is the predominant solid-based technique. In LOM, solid objects are processed to have a laminate covering. The biggest area of AM is the powder-based techniques. Powder-based techniques are primarily sintered, bound under high pressure, or bound with an adhesive. Although more current versions of these techniques are used in tissue scaffolding, the fundamental technology is the same.

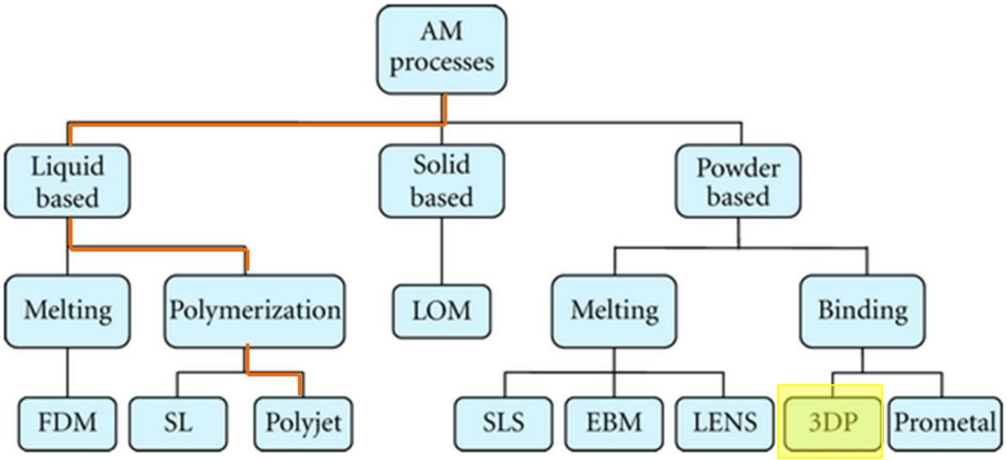

Figure 9. Three-dimensional printing processes highlighting that 3DP is now synonymous with AM and that currently 3DP encompasses more than powder based techniques [25] (reprinted with permission from Hindawi Publishing Corporation).

Stereolithography was one of the first AM techniques. The desired prototype is formed from a bulk liquid solution. A laser precisely polymerizes the structure layer by layer, and the remained liquid solution is washed away. Inkjet technology prints a continuous filament that adheres to a substrate. The advantages of direct ink write printing, a subset of inkjet printing, are described in the next section.

2.4 Advantages of Direct Ink Write Printing

Table 3 shows a comparative analysis of successful scaffolding techniques. There are four different types: inkjet, electrospinning, extrusion based, and lithographic methods. With the exception of electrospinning, each technique utilizes computer-controlled layer-by-layer deposition. Electrospinning creates a fiber mesh that is very useful for creating highly porous interconnected networks. The strength of DIW printing is based on its simplicity. There are no extra masks or support structures, no use of high temperatures or pressures, and no use of a bulk polymer solution that leaves residue.

Table 3. Summary of applicable scaffolding methods

Printing	Defining Characteristics	Pros	Cons	Reference
Direct Ink Write (DIW)	Layer-by-layer deposition of slid viscous filament at a constant rate. Extrusion based on CAD.	Under ambient conditions good for cell seeding	Resolution limited to 50microns UV curing post-extrusion needed	[3]
Electrospinning	Voltage draws out fibers to form a mesh	Great resolution and highly interconnected network	Uncontrollable fiber deposition, poor mechanical strength	[26, 27]
Fused Deposition Modeling (FDM)	Polymer ink is heated and forced through extruder	Excellent control, layer separation, and resolution	High temperatures and pressures needed	[28]
Stereolithography (SL)	Light used to form structure from a photopolymer solution	High resolution complex structures	Only photopolymers Irradiation harms cell growth	[3]
Two Photon Lithography (TPL)	Powder solution is sintered to for an architecture layer-by-layer	No post processing needed, self-supporting,	Specific masks and additional support materials needed	[4]
Selective Laser Sintering (SLS)	Layer-by-layer construction from a powder bed	No support features and post processing needed	Resolution limited to laser beam, high temperatures used	[4]

2.5 Introduction to Tissue Engineering

The first step to creating a 3D printed tissue is to image the designed tissue. Tissue engineering aims to renew unhealthy tissues in the body by combining a supporting structure (scaffold) with healthy cells. In a review article, Melchels et al. revealed the powerful potential of AM to revolutionize the field of TE in the upcoming years [4]. AM, as stated above, creates a 3D object by layer-by-layer deposition using a CAD. AM prototyping uniquely stands to impact regenerative medicine in the realm of turning digital images of implants into tissues and organs. The 3DP body parts are developed using the patient's cells which therefore producing individualized patient care on a large scale. Figure 10 displays an idealized AM process: MRI of breast tissue, AM scaffolding with cells suspended in printing ink, vascularized breast implant, and breast implant after mastectomy. Many difficulties have prevented this model from becoming an actual implant. The cell embedded gel must pass through a nozzle and retain a stable shape while maintaining cell life and promoting cell growth. Currently, scaffolds have been made that aid in repairing bones, cartilage, and skin, but this structure has lacked incorporation of patient cells. Vascularization, biocompatibility, and biodegradation depend heavily on the material selected for the cell matrix.

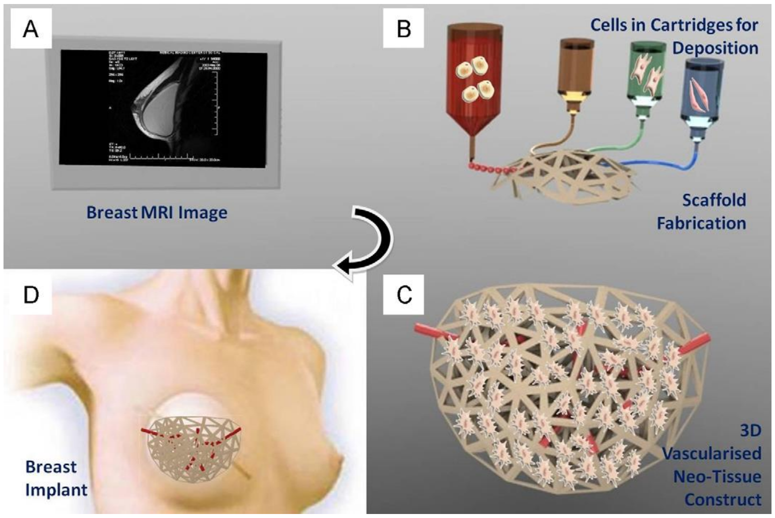

Figure 10. Bioscaffolding design processes. An MRI image of a breast tissue. The MRI is used to generate a CAD breast implant design in b. The multiple cell types are loaded into ink cartridges and used to create a vascularized tissue construct as seen in c that will be implanted as seen in d [10] (reprinted with permission from Elsevier).

There are currently clinical problems with organ transplantation. In the U.S., there are 100,000 patients on the waiting list for organs. The waiting time can be years, and many patients die from organ failure while waiting. Future options will be to grow one's own organs in an incubator or to print one's own organs. Ott expanded the field of TE by growing functioning rat hearts, lungs, and kidneys from cadaveric tissues [5, 17, 29]. Bayley pioneered printing organs from lipid bilayer droplets to have a reported elastic modulus of 100 to 200 kPa. The discoveries from the research groups demonstrate the viability and potential applications of TE.

2.6 Common Materials Used for Tissue Engineering

The following is a brief list of the most commonly used polymer to make hydrogels: Poly(caprolactone) PCL, Collagen, Hyaluronic Acid (HA), Poly (ethylene glycol) PEG, Pluronic F-127 (F-127), Poly (methmethacrylate) (PMMA), and poly(lactic-co-glycolic acid) PLGA.

Hydrogels are crosslinked polymer networks that hold water and form the inks used in tissue scaffolding. Water sustains cell growth and the ability of the polymers to hold water aids in biodegradability. These materials are used for their variability of strength, durability, biocompatibility, porosity, insolubility, temperature stability, functionality, and ability to encapsulate cells. Reproducible results are limited in studying viscoelastic materials. Gilbert et al. (2013) defined a four step protocol to ensure reproducibility [30].

Hydrogels have a variety of applications as biocompatible materials capable of being integrated with the body. Their use extends from contact lenses to biosensors, controlled drug release, wound healing, and, now, tissue scaffolding [15, 31]. Hydrogels are well suited for TE because they are able to retain a large percentage of water which creates an environment similar to live tissues. The Zandstra Lab used Atomic Force Microscopy (AFM) to characterize the elastic modulus of common cell types. The results of their work can be seen in Figure 11. Soft tissues such as brain and fat tissues are below 10kPa. In their studies, they found that cells such as fibroblasts attach to stiff matrices of 20kPA or higher [32].

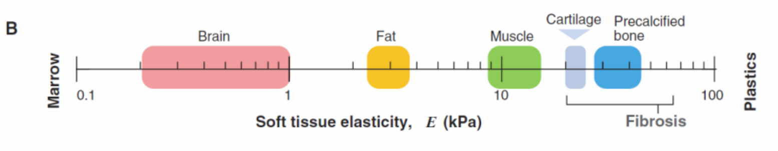

Figure 11. Elastic Modulus of common soft tissue type found using Atomic Force Microscopy [32] (reprinted with permission from Royal Society of Chemistry).

Table 4. Comparison of biomaterials for tissue scaffolding. Compiled from [12, 23, 29].

Polymer	Structure	Modulus (kPa)	Scaffold Type
Poly(1,8-octanediol citrate) POC	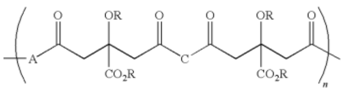	Elastic 2,000-14,000	Cartilage
Hydroxyapatite (HA)	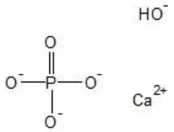	Elastic 150,000 Shear 0.001	Hard Bone
Poly Lactic Acid (PLA)	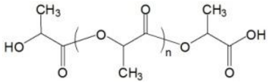	Elastic 3750	Soft Tissue
Chitosan	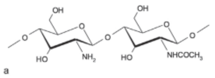	Shear 0.01	Bone
Poly Methylmethacrylate (PMMA)	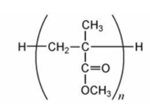	Elastic 18,000-31,000	Hard Bone
20 kDa Poly(ethylene glycol) PEG	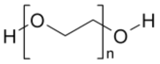	Elastic - 0.06	Muscle Cartilage
23wt% Pluronic F127	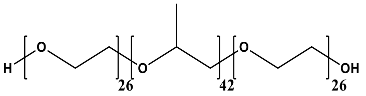	Shear 0.01	Soft Tissue

Polymers such as POC, HA, and Chitosan form hard rigid scaffolds that are very compatible with bone and cartilage tissues. Polymers such as PEG, PA, and PDMS form great ECM materials, but are not used as scaffolding materials due to toxicity concerns. However, PEG at high MW is not toxic, but the ester linkages may decompose into shorter chain PEGs that are unsafe. Pluronics, especially F-127, form micelles slightly below room temperature which help to give their hydrogels added support.

Mechanical properties like stiffness and strength of alginate gels can be controlled by physical factors. Concentration of polymer and its molecular weight can be used to determine the density of polymer solution for formulation of gels. Increase of both these factors leads to higher viscosity of the polymer solution and hence a stiffer and mechanically strong gel. Cationic poly (ethyleneimine) (PEI) additionally leads to improvement of alginate gel's mechanical properties. High-molecular-weight PEI increases the resistance of the gel to de-crosslinking agents and thus improves the gel's stiffness. Gelling conditions such as temperature, type, and concentration of cross-linker also affect the mechanical properties of alginate gels. Low-temperature cross-linking leads to slow cross-linking, due to reduced rate of calcium ion diffusion. This results in the formation of gels with enhanced mechanical properties. Apart from these factors, the presence of cells in the gels is also shown to improve its mechanical strength.

Tensile test is the basic characterization of mechanical properties of a given polymeric biomaterial. Tensile strength is important for polymers used in repairing cartilage and ligament ailments. Desirable values of the parameter can be achieved by altering the degree of crystallinity of the polymer and by controlling the orientation of fibers during electrospinning. For instance, elongation at break of biodegradable scaffolds made of poly (p-dioxanone) fibers used for cartilage TE can be controlled by aligning the fibers along a certain direction using a dynamic collector in electrospinning. A two fold increase in elongation at break was observed between random and aligned fibers.

In addition to the porosity and mechanical strength, swelling is an important factor when evaluating a material for TE applications. Pollock et al. studies the swelling behavior for PEG, F127, and F68 hydrogels as seen in Figure 12. They found that swelling occurs more at lowered temperatures and in Pluronic hydrogels rather than PEG hydrogels with higher EO% Pluronics absorbing over 3.5 times their original weight.

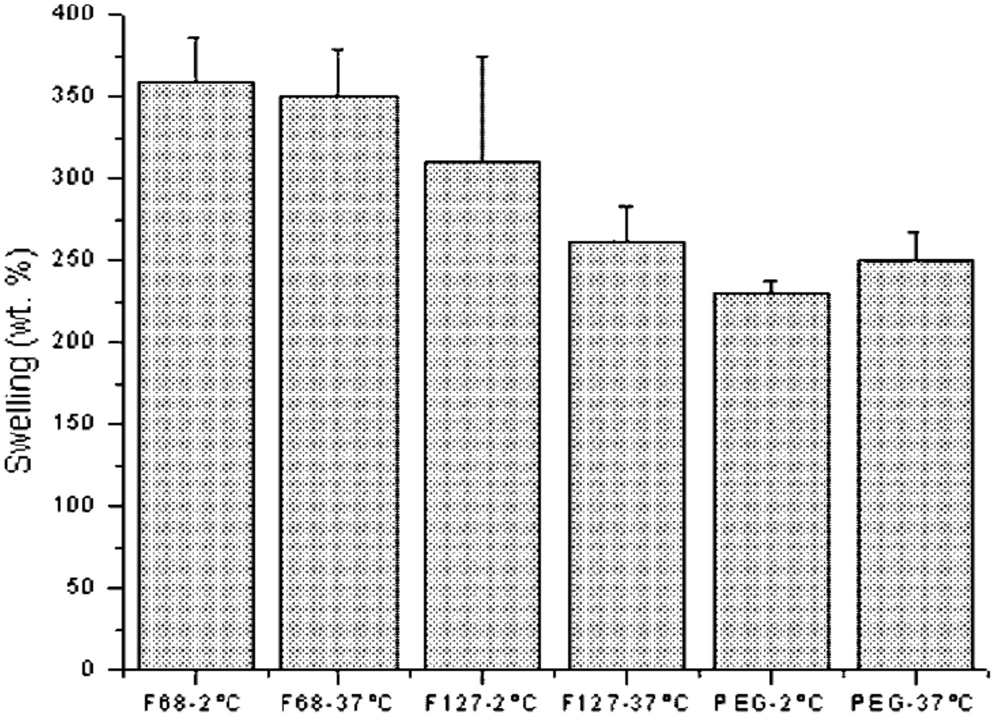

Figure 12. Swelling of F68 (40 wt.-%), F127 (20 wt.-%), PEG3400 (20 wt.-%) after 5h [33] (reprinted with permission from Elsevier).

2.7 Results of Scaffolding

This section discusses the scaffolding results of via SLS, FDM, and DIW printing methods. Extrusion based techniques require a calibration nearly every time printing occurs. The Lewis group varied the write speed and write pressure separately to determine the parameters that generated the similar filament to nozzle diameters as seen in Figure 13. This calibration technique will be applied to the experimental procedures. Selective Laser Sintering (SLS) has been applied to TE to porous scaffolds capable of

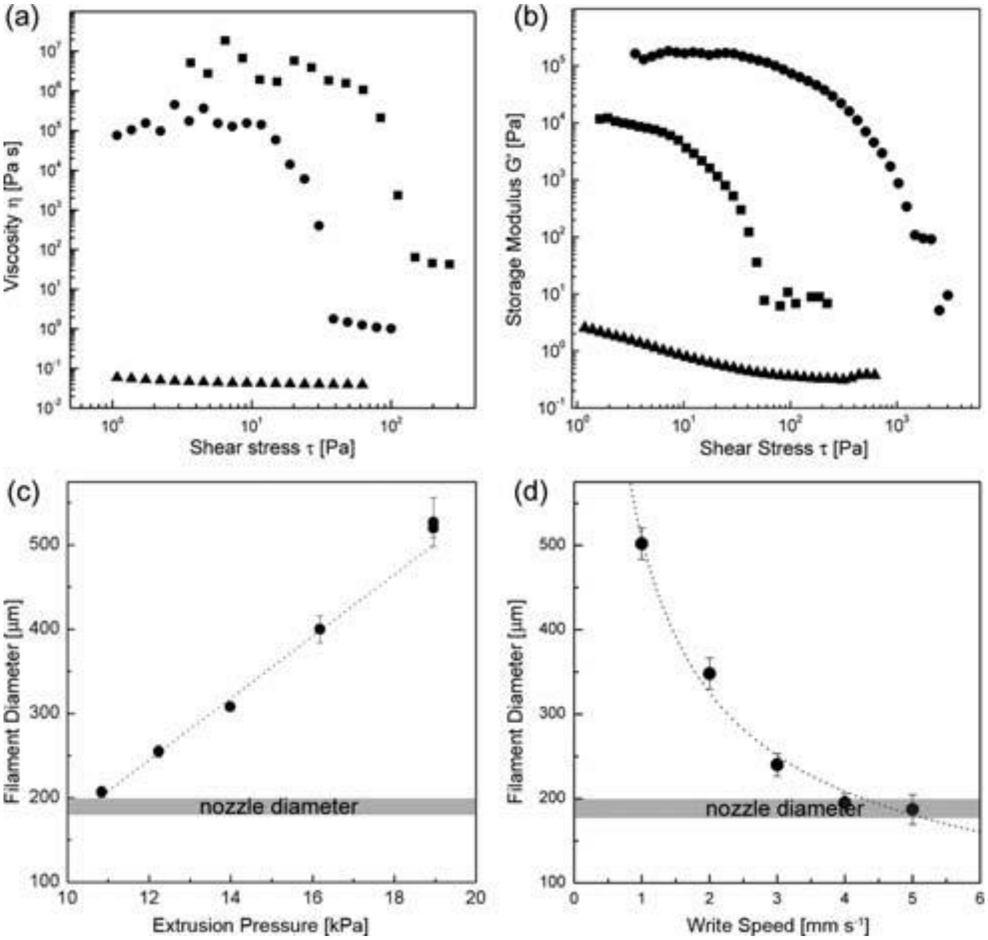

Figure 13. Printing optimization by varying write speed and pressure [16] (Reprinted with permission from Applied Rheology).

growing bone and cartilage tissue. Partee et al. used polycaprolactone (PCL) powder under the brand name CAPA® 6501to fabricate miniature pig and human condyle scaffolds. The scaffolds made by SLS have high surface porosity but the resolution is limited to the scan spacing and powder lay delay time which resulted in blurred edges. The results of the scaffolding types are fairly consistent with changes in resolution, size, and possible shapes. Figure 14 shows different fabricated geometries and various

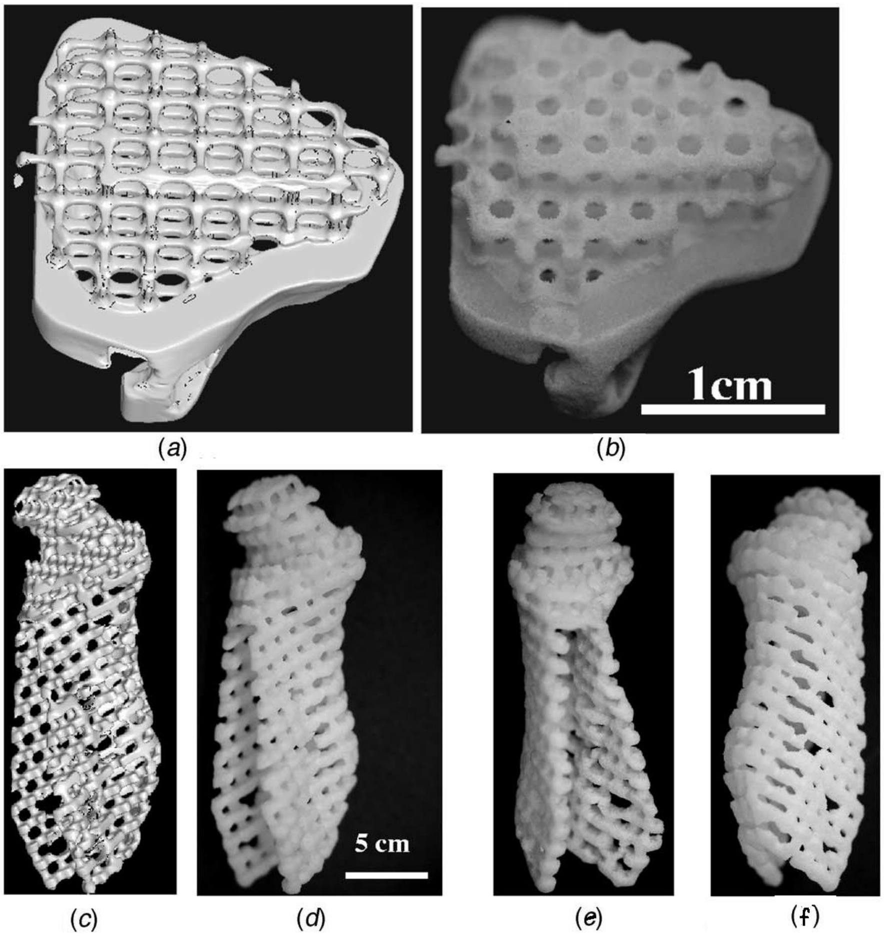

Figure 14. CAD designs followed by the physical SLS model of PCL scaffolds. a and b) Minipig mandibular condyle scaffold. c-f) Human condyle scaffold [34].

porosities of PCL printed via Fused Deposition Modeling (FDM). Each geometry in Figure 15a has extremely high resolution. Figure 15b displays the cross-sectional area of the typical woodpile structure of a freeze dried sample. Using FDM the porosity can be varied according to the spacing between each layer. A closer look at the structure reveals that FDM is one of the most precise 3DP methods. Using inkjet and DIW techniques, printing various patterns with cells integrated into the ink has been proven possible.

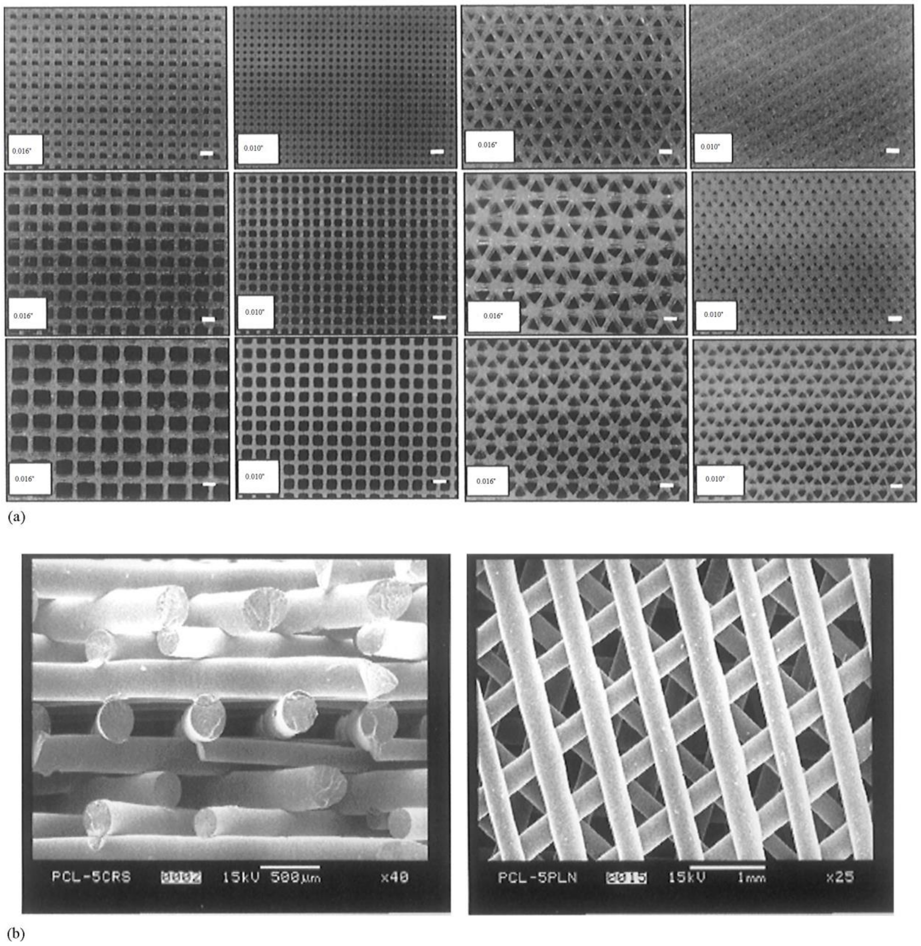

Figure 15. Various scaffold structures of PCL printed via FDM from a) 406 to 254 μm with nozzle diameter listed. b) Woodpile structures revealing near perfect layer separation [35] (reprinted with permission from Elsevier).

Figure 16 shows the scaffolding results for DIW printing methods. The deflection under atmospheric loads can be seen in Figure 16 for a particle-filled ink and 40 wt% microcrystalline organic wax. Figure 16c shows the time stabilization of the deflection. The structure began to stabilize at 2h and sagged a total of 8mm. Sagging and spreading filaments are unique to DIW and inkjet printing techniques. When printing multilayered structures, selecting materials with higher G' values is crucial and helps to increase the resolution of the interconnected networks. A 104 layer scaffold was fabricated using particle-filled organic ink as seen in Figure 16d, and the same structure was placed in an epoxy in 16e. The surface of a scaffold needs to be porous along with the porous interconnected networks. Figure 17 shows the surface of an hyaluronic acid (HA) scaffold at 200x magnification and 15000x magnification. Surface porosity is vital to hold moisture and nutrients for cell cultures. Each structure will have significant surface porosity that can be correlated to the swelling of the material in an aqueous solution.

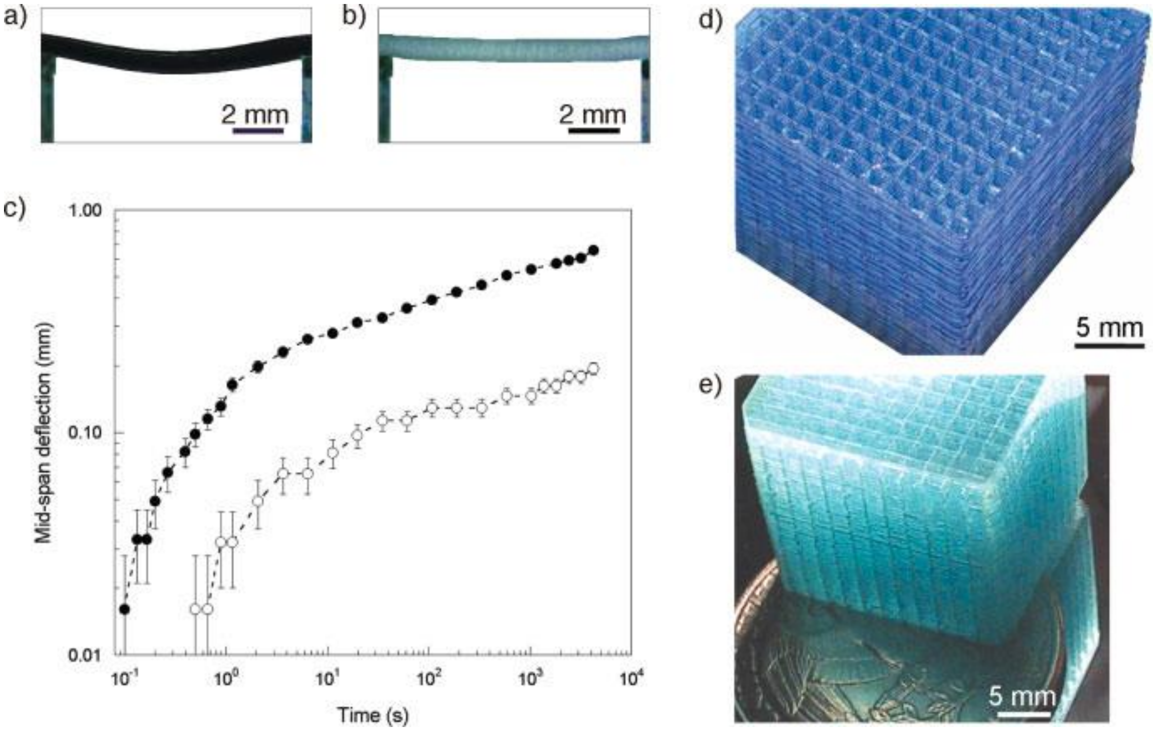

Figure 16. Optical images of the side view of the span of organic ink filaments a) particle filled ink and b) microcrystalline wax ink. c) Span deflection and c) d-e) layered structure of particle filled and microcrystalline wax ink with a quarter to show scale [17] (reprinted with permission from Elsevier).

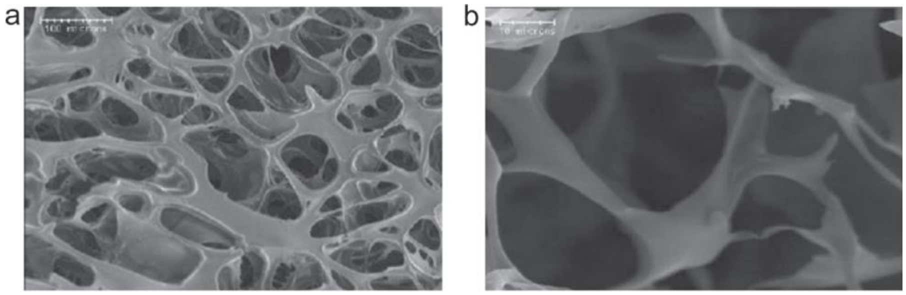

Figure 17. SEM image of the surface of the HA scaffold revealing the surface porosity [36] (reprinted with permission from Elsevier).

2.8 Disadvantages of Pluronic F-127

Microvascular networks occur in every biological system from multi-branched networks in leaf stems to the intricate circulatory system OF HIGHER ANIMALS. Although the networks are long, the channel diameter was found to be 10μm [23]. The material weaknesses become apparent at extremes like this. Hydrogels, specifically Pluronic F-127, are severely limited in strength, shape retention, and degree of photopolymerization due to chain interactions. Hydrogels, in general, very easily crack and degrade over short periods of time. W. Wu et al. circumvented the weaknesses of F-127 by direct write printing into a low viscosity epoxy resin also known as an extracellular matrix (ECM). The epoxy resin served to provide shape and structure to the printed material. The benefits of using an ECM are maintained use of materials that extrude smoothly and easily print. Once printed in an ECM, F-127 must be removed to create microvascular networks. Pluronic F-127 liquefies when cooled which simplifies the cleaning process. Another concern is the ability to crosslink under UV light. Pluronic F-127 has been shown to have only a slight increase in stiffness. Because of its low G' F-127, arguably, is not suited as a scaffolding material for a range of different tissue types.

2.9 Waxy Ink Alternative

This project focuses on the properties necessary for a material to serve as an ink for 3D printing of scaffolds for TE. A foundational overview of the mathematics and physics behind polymeric liquids is provided to aid the understanding of materials characterization. Pluronics are the ideal candidate for 3D printing due to their biocompatibility, range of mechanical strengths, and ease of functionality. Similar to hydrogels, waxes can be used as inks for 3D printing and tissue scaffolding. Pluronic F-127 has been used to create microvascular networks by direct write printing into an ECM. Kolesky et al. extensively researched the vasculature needed for successful cell growth that can be created using F-127 [13] [13]. Pluronic F-127 liquefies when cooled due to the relaxation of entangled chains known as micelles that exist at room temperature. Using the low temperature-induced structure change of F-127, Kolesky et al. constructed a multi-materials ECM with a cell-laden micro-engineered gelatin methacrylate hydrogel (GelMA) printed with the desired vasculature as seen in Figure 18. The materials used were polydimethylsiloxane (PDMS), Pluronic F127, and two different cell laden GelMA inks. Pluronic F-127 was printed into a PDMS ECM, then washed away by cooling the mixture. The remaining hollow channels creased interconnected networks to promote cell growth. Forming intricate cell links and connectivity using waxes has many difficulties that may result in limited use to create sustainable cell growth.

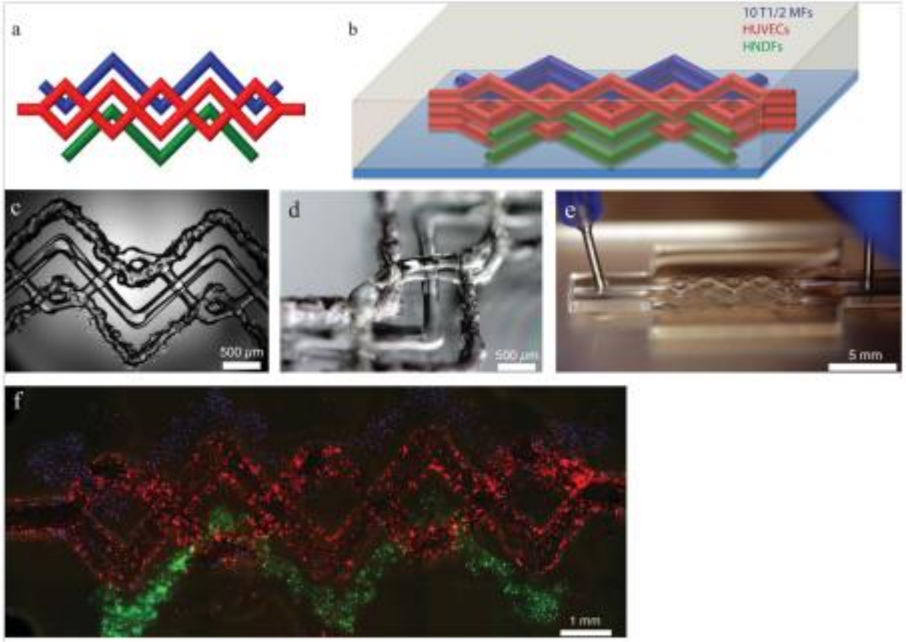

Figure 18. Design and printing process. a, b) 1D depiction to CAD of vasculature with different dyes representing different cells lines. c-e) 3DP GELMA cell-laden constructs. f) Flourescence image of the growth of cells [13] (reprinted with permission from John Wiley and Sons).

The Lewis group demonstrated that microcrystalline waxes could also be used to create microvascular networks. The waxes liquefy with increased temperature, so the cleaning process is reversed to remove the material from the ECM. Unlike hydrogels, waxes do not readily lose moisture or crack. Waxy inks also mold to the shape of a syringe and retain the shape long after extrusion, and their already strong mechanical properties can be doubled with photopolymerization. Several of the properties make wax an ideal candidate as a TE scaffold. While the advantages to using a wax seemingly outweigh hydrogels, the overall success of waxes as a cell growth medium is unexplored. Waxes need protein modifiers ingrained into the ink structure to attach cells. West et al. [37] used a peptide called KQAGDV in a PEGDA hydrogel to successfully attach human dermal fibrolasts (HDF). The cells proliferated through the scaffolding structure and remained 95% viable post photopolymerization for 7 days.

Other challenges in using waxes include lack of research correlating write speed, syringe diameter, and rheological studies. Figure 18 displays subsequent research that would need to be conducted to bring waxes closer to use as cell implanted scaffolds. The first step is to establish the capability of printing CAD structures using waxy inks. Although stronger mechanical properties limit waxes, blending the material with softer polymers could yield favorable results. The Lewis Group optimized all of their studies for F-127 at 23wt% in 76wt% water. Introducing a softening agent such as a solvent or miscible liquid polymer has been shown to decrease the strength of the organic waxes.

2.10 Summary

Three dimensional tissue scaffolding is still in its nascent stages. Research is still needed to establish the important variables for success of tissue growth and regeneration. Although the Lewis Group at Harvard University has pioneered the field of 3D printing to investigate many of these parameters, no functioning organs have been printed. The previous work presented in this paper has established the foundation for more work to be done.

Ranges for the elastic and loss moduli and viscosities of starting materials were appropriately identified in these two articles. A technique for printing microvascular networks was also developed. Because Pluronic F127 forms a weak gel, the Lewis Group compensated for this inefficiency by printing in a gel matrix and went on to successfully print a complex microvascular network.

Rheological studies were crucial to this research and will continue to be a vital part of research into 3D printing. Without understanding the viscoelastic properties of the material, it may be near impossible to find a material that is strong enough to independently retain its shape while shear thinning to allow flow through a needle.

Rheological studies are crucial to this field due to the ease of testing. Once the LVR is established and the frequency of testing is set, gathering data can be nearly automated. Future work is needed to determine more about the printing mechanics and the long term validity of these results.

CHAPTER THREE

RESEARCH OBJECTIVE

The objective of this research was to study the complex viscosity of Pluronic P85 and Jeffamine ED 2003 formulations with a goal of correlating rheological data to the printing behavior. The storage modulus and yield strength of the starting ink material influence the printing behavior. Thus, the major objective of this research is to explore several avenues to find the elastic and shear moduli and investigate any relationship between the moduli and the pressure to start and continue flow within a syringe.

Typically, biocompatible inks that could be used for DIW printing are too soft. One way of harden them is to add photocurable side groups that enhance the stiffness of the material by forming cross linked polymer networks. The proposed materials are easily functionalized with acrylate groups following the Cellesi protocol [38]. The added benefit of using strong starting materials will be tested and quantified, and the printing behavior will be documented. The results of this research will be to design extracellular matrix scaffolds that could be used for tissue cell growth and separation.

CHAPTER FOUR

MATERIALS AND METHODS

4.1 Diacrylate Endcap Synthesis

Three-dimensional inks are made from polymer materials with desirable mechanical properties. Poly (ethylene glycol) and poly (propylene glycol) block copolymers known as pluronics (BASF trade name), and poloxamers (ICI trade name) have widespread use in TE as scaffolding materials. Pluronics are primarily used for their biocompatibility and their amphiphilic behavior which allows them to operate undisturbed in the body. Pluronic F127 is the most popularly used Pluronic due to the temperature and concentration dependent gelation. Many research groups have printed extracellular matrices using F127 that have successfully sustained mesenchymal stem Cell (MSC) growth. Other block copolymers such as Pluronic P85 and Jeffamine ED 2003 have a higher storage modulus (G') in addition to similar amphiphilic behavior and biocompatibility. A higher G' translates to a stiffer material that is self-supporting. Other materials were functionalized to compare to the published results on F127.

4.1.1 Free Radical Polymerization

Free radical photopolymerization of the Pluronic starting materials became one of the many necessary steps to accomplish printing 3D structures. Adding a cross-linkable side group was hypothesized to have two added benefits. First, the change would preserve the original properties of the material (e.g. the shear thinning behavior) while preparing the material to permanently retain its shape after extrusion. The reaction route to preparing a UV curable printing ink originated from Cellesi et al. as seen in Figure 19

[38]. They targeted Pluronic F127 to be part of a multi-component thermal gelation and covalent crosslinking human foreskin cell encapsulation technique for cell transportation therapies. As a result, they developed a one-step method for replacing the terminal hydroxides with UV curable acrylate end groups.

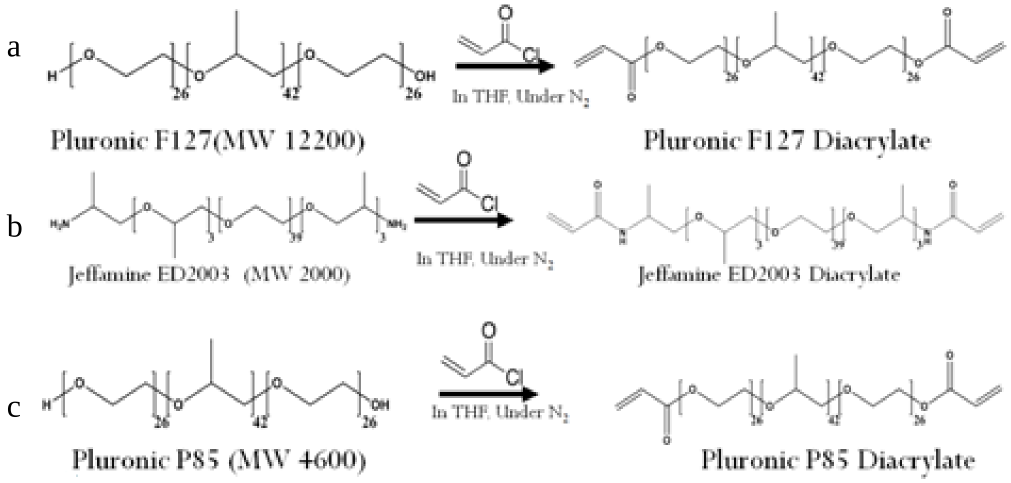

Figure 19. Diacrylate functionalization chemical synthesis route of a) Pluronic F127 b) amine terminated Jeffamine ED2003 and c) Pluronic P85. All Pluronics, Tetronics, and commercially available starting materials were functionalized with this reaction.

Commercially available pluronics and jeffamine (chemical structures seen in Table 5) were first azeotropically dried using toluene, cooled to room temperature, and rotovapped to remove the solvent. The starting polymer was then re-dissolved in 15mL of THF per gram of polymer and mixed first with triethylamine, then acryloyl chloride, both in 2.5 molar equivalents per OH group. The reaction was cooled with an ice bath and stirred under N2 overnight. Triethylamine acts as a base to remove the hydrogen from the terminal hydroxide groups priming the starting polymer for a substitution reaction with the carbonyl to replace the acyl chloride on acryloyl chloride resulting in a free chloride ion. The addition of the acryloyl chloride turns the solution cloudy which can be attributed to the formation of triethylammonium chloride salt. The final product was purified by filtration, liquid—liquid extraction in DCM, and dried using magnesium sulfate then rotovapped to remove any remaining solvent.

4.1.2 Proton NMR Results

A proton nuclear magnetic resonance (NMR) was performed on a Bruker Avance 500 instrument at 400 MHz using polymeric samples dissolved in CDCl3 (deuterated chloroform). δ 1.2 (133H, d), 3.6 (328H, m), 3.75 (204H, m), 4.35 (4H, t), 5.8-6.5 (6H, m).

Table 5. Company origin and chemical formula of commercially available starting materials

Polymer	Chemical Formula	Company
Pluronic L121	$HO(CH_2CH_2O)_5(CH_2CH(CH_3)O)_{68}(CH_2CH_2O)_5H$	BASF
Pluronic P85	$HO(CH_2CH_2O)_{26}(CH_2CH(CH_3)O)_{42}(CH_2CH_2O)_{26}H$	BASF
Pluronic F127	$HO(CH_2CH_2O)_{100}(CH_2CH(CH_3)O)_{65}(CH_2CH_2O)_{100}H$	BASF
Tetronic 1301	$(HO(CH_2CH_2O)_4)_2((CH_2CH(CH_3)O)_{27})_2NCH_2CH_2N ((CH_2CH(CH_3) O)_{27})_2 ((CH_2CH_2O)_4)_2H$	BASF
Jeffamine ED 2003	$NH_2CH_3CHCH_2(OCH_2CHCH_3)_3(OCH_2CH_2)_{39}(OCH_2CHCH_3)_3NH_2$	Huntsman

The functionalization reaction was verified by two distinct methods, proton NMR and UV curing. A representative spectra of P85DA revealed the formation of several small downshifted multiplets that correspond to the six hydrogen atoms found on the terminal alkene as seen in Figure 20. The Cellesi group reported a 100% conversion of the hydroxide groups to acrylate groups and a yield of 80% for F-127. The conversion and yield are listed for a representative sample of starting materials in Table 6. Of the solid, paste, and liquid starting polymers, pastes such as P85 and Jeffamine ED2003 had higher yields while liquids such as L121 had the lowest yields and conversion rates as seen in Table 6.

Table 6. Resulting change in MW, typical degree of functionalization, and typical yield of diacrylate reaction of representative samples

Polymer	Original MW	MW Difference (%)	Average Conversion	% Yield
Pluronic L121	4400	2.0	70	75
Pluronic P85	4600	1.9	95	84

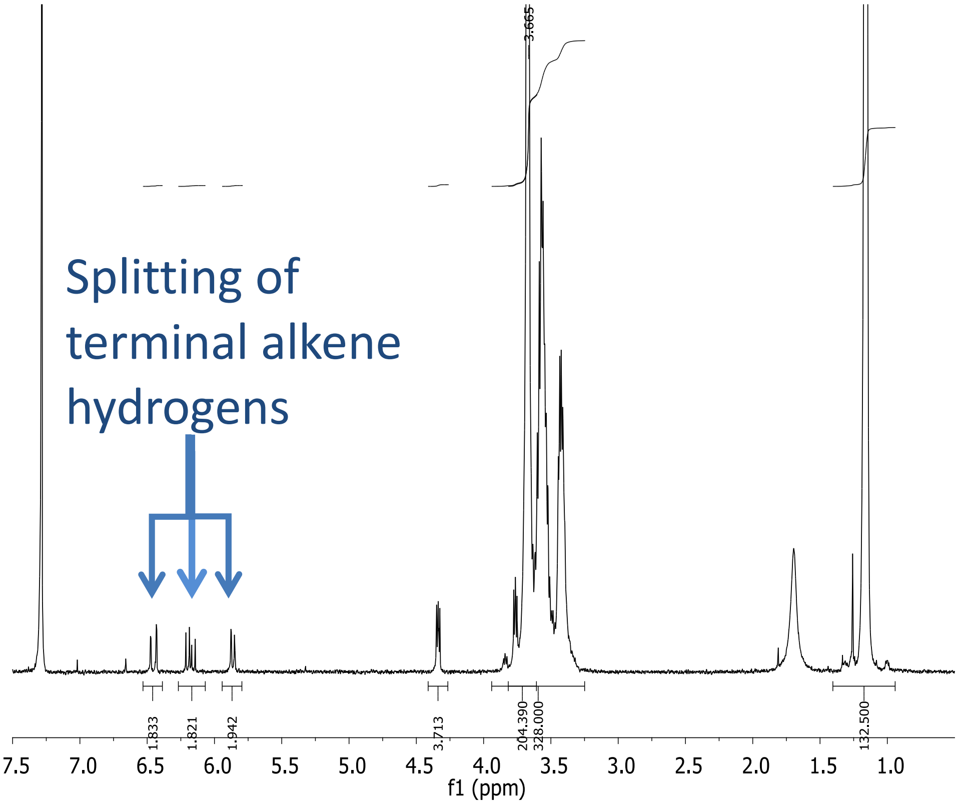

Figure 20. Proton NMR of Pluronic P85DA executed by (1H NMR) was performed on a Bruker Avance 500 instrument at 400 MHz

4.1.3 Ultraviolet Curing Test

The second step for evaluating the presence of acrylate end groups was a quick visual test for photopolymerization. Initial formulations were designed to develop hydrogels that experienced an increase in viscosity due to photopolymerization. Acrylates undergo free radical polymerization to form cross linked polymer networks that can result in a rigid hydrogel. Initial photopolymerization experiments were performed at room temperature in deionized water with 1wt% photoinitiator (Irgacure 2959). The following weight percent (wt %) solutions were prepared to form a hydrogel: 5 wt%, 10 wt%, 25 wt%, and 50wt%. Then each solution was exposed to 300 nm UV light for 20 min.

4.2 Ink Preparation

A two-step method was used to prepare the 3DP inks: functionalizing the hydroxyl groups to photocurable acrylate groups, and formulating the inks by mixing together a hard paste with a softer material.

4.2.1 Ink Formulation Methods

After the acrylate end-capping synthesis, the UV curable polymers were mixed. Pastes with a higher stiffness (G') such as P85 and Jeffamine ED 2003 were mixed with liquid Pluronics to soften the overall structure and lower the yield stress. Also a small weight percent of Darocur 1173 photoinitiator was added, sealed in a vial with Teflon tape, then sonicated at 60^{o}C for 1h. While warm, the mixture was poured into the ink supply syringe barrel, then cooled and sealed. An overview of the formulation process can be seen in Figure 21. The experimental matrix for polymer formulations can be seen in Table 7. The complex viscosity was found using a dynamic oscillatory shear stress via parallel plate rheometry. The percent ethylene oxide (%EO) content was found by calculation based on the chemical structure.

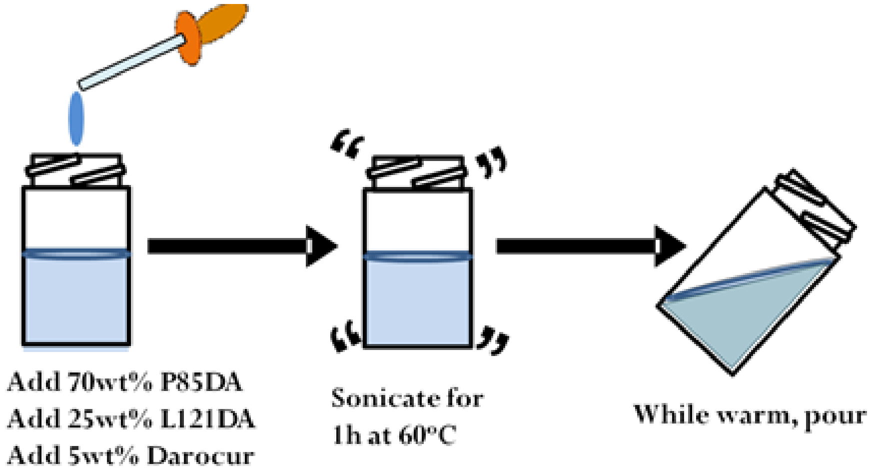

Figure 21. Example formulation process to develop printing inks.

Table 7. Printing studies matrix of formulations.

Type	η* [Pa•s]	Component 1	wt%	Component 2	wt%	%EO Mixture	Total MW
Pluronic	19400	P85	0.7	L121	0.3	0.38	4540
Pluronic	23650	P85	0.8	L121	0.2	0.42	4560
Jeffamine	7430	JAED 2003	0.3	L121	0.7	0.331	3680
Jeffamine	7430	JAED 2003	0.35	L121	0.65	0.3695	3560
Jeffamine	NA	JAED 2003	0.5	L121	0.6	0.408	3440
Pluronic	3403	P103	0.3	P123	0.7	0.3	4425
Pluronic	590	P103	0.4	P123	0.6	0.34	4500
Pluronic	3403	P103	0.3	P105	0.7	0.5	6035
Pluronic	8307	P103	0.5	P105	0.5	0.4	5725
Tetronic R	4.65	JAED 2003	0.2	90R4	0.8	0.494	6192
Tetronic R	345	JAED 2003	0.4	90R4	0.6	0.588	5144
Pluronic R	409	10R5	0.3	P85	0.7	0.5	3805
Pluronic R	88	10R5	0.2	P85	0.8	0.5	4070
Tetronic R	4750	P85	0.65	1301	0.3	0.38	5260
Tetronic R	2027	P85	0.8	1301	0.15	0.42	5040

4.3 Instrumentation

Overall, the materials used as ink in this work were evaluated by the methods shown in Table 8. The physical characteristics were calculated using tensile and shear tests, i.e. TA Instruments 2980 model DMA and rheology, while the chemical structures were verified using proton nuclear magnetic Resonance (^{1}H NMR) performed on a Bruker Avance 500 instrument at 400 MHz using polymeric samples dissolved in deuterated chloroform ($CDCl_3$). The porosity was understood by comparative analysis of the swelling content. Finally, the thermal degradation behavior was quantified using a TA Instruments Q500 model thermal gravimeric analysis.

Table 8. Summary of characterization techniques by desired property

Material Property	Characterization Technique
Mechanical behavior	
Storage/loss (elastic and shear) moduli Crosslink mesh size and density	Dynamic mechanical analysis, rheology swelling tests in distilled water
Chemical Analysis	
Chemical Structure and composition	Nuclear magnetic resonance
Porosity	
Pore size and morphology	Swelling and microscope imaging
Thermal Analysis	
Degradation temperature	Thermal gravimetric analysis

Each unique ink formulation is tested using parallel plate rheometry on an AREX 2000 Rheometer at 25°C as seen in Figure 22. The rheometer calculates the storage moduli G', loss moduli G”, and complex viscosity η* over increasing shear stress. Each sample was taken within the Linear Viscoelastic Regime (LVR) with a frequency of 1Hz.

Figure 22. TA Instrument AREX 2000 parallel rheometer with parallel plate geometry and thermal control using a peltier plate.

The DIW printer set-up is shown in Figure 23. The printing studies will be done on the DIW set-up at IBM Almaden. The translation stage is controlled with MATLAB software. The syringe is loaded while the polymer is in the melt form. After cooling, the samples are used to construct different geometric patterns. The first test is printing four sets of six lines. The first set is to obtain consistent flow of material. The second and third are to optimize the pressure and write speed. The final set tests the optimization parameters. After this calibration, the sample is ready to print more complex geometries. The ink supply is distributed via an air pressure dispensing system. The z-axis is independent of the x and y axes in that the ink supply has a separate z-axis motor while the platform moves in the x and y direction. There is a Thorlabs 365nm, 27 W/cm² UV lamp present to perform in situ curing if needed.

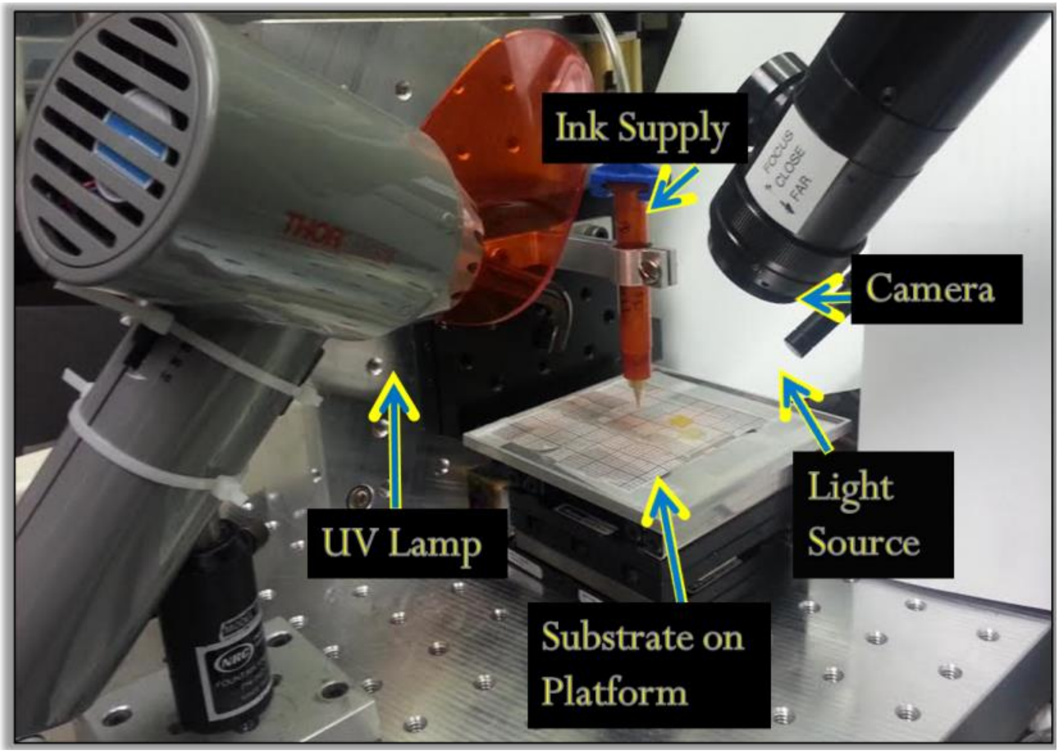

Figure 23. Experimental set-up of DIW printer. PERSONALLY TAKEN PHOTOGRAPH: Allen, A'Lester. "Experimental set-up of DIW printer." 2014. jpeg.

Tensile strength and percent elongation at fracture of the pluronic specimens was tested using an Instron tensile tester as shown in Figure 24 and following ASTM D 638. A 10N load cell was chosen for the Instron tester. However, the only clamps available for use fit on the 50kN load cell. Due to this, the 50kN load cell was used for the following tensile tests.

Figure 24. Instron tensile tester in Engineering Room E105 at San Jose State University. PERSONALLY TAKEN PHOTOGRAPH: Allen, A'Lester. "Instron tensile in Engineering Room E105 at San Jose State University." 2014. jpeg.

CHAPTER FIVE

RESULTS AND DISCUSSION

Presented here are the results of a series of experiments designed to find a range of characteristics associated with a suitable scaffolding material to use as an ink for 3DP. The first set of experiments evaluated the use of F-127 hydrogels to fabricate self-supporting scaffolds. Pluronic F-127 was unable to be used as a standalone material, so the next set of experiments investigated the use of organic wax (OW). Successful printing determined that OW can be used as a trial substance to determine the material properties (G', η^*, τ_y) that are needed to obtain ease of printing, layer separation, and self-supporting scaffolds. Next, a class of triblock copolymer pastes were used to formulate an ink similar to OW. The results below detail the challenges, success, and characterization of each step and the successful biocompatible inks.

5.1 Analysis of F127

Pluronic F127DA was expected to have an increase in viscosity after UV exposure due to the formation of a cross-linked polymer network; however, there was no visible change in viscosity after the concentration dependent gelation at 25wt% [14]. Subsequently, tests to evaluate the effect of molecular weight and ethylene oxide (EO) to propylene oxide (PO) ratio were performed on four test specimens: 8000 MW PEGDA, 6000 MW PEGDA, Jeffamine ED 2003DA, Pluronic F68DA.

5.1.1 Evaluation of Functionalization Reaction

Poly (ethylene glycol) Diacrylate PEGDA is known to form a solid cross linked network upon UV exposure [39]. To control for the effect of molecular weight, two samples of 8K PEGDA and 6K PEGDA were used at the same concentrations as F127DA. There was no effect on the viscosity of the hydrogel of the 8K PEGDA specimens, but all of the 6K PEGDA specimens formed a cross linked network that resulted in a solid hydrogel. This indicated that there was a MW constraint to forming solid hydrogels. The same tests were performed on Jeffamine ED 2003DA and Pluronic F68DA, which both have a higher EO/PO ratio. Jeffamine ED 2003DA has an average MW around 2000amu, while F68DA has a higher average MW around 8350amu. Jeffamine ED 2003DA did not form a viscous hydrogel, but post UV exposure, each concentration formed a solid hydrogel. Figure 25 shows a summary of the initial F127 curing results.

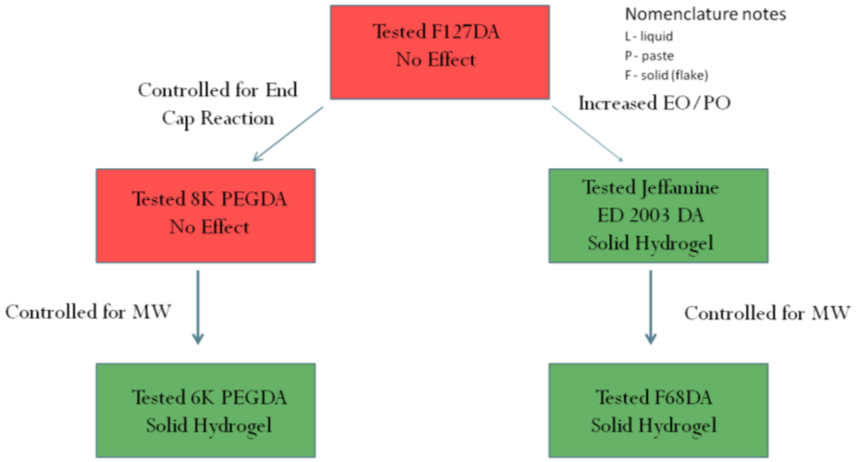

Figure 25. Pluronic F127 curing results and determining parameters to form a robust hydrogel.

5.1.2 Robust Hydrogel Definition and Summary of UV Curing

Pluronic F68 formed a viscous hydrogel at every concentration and formed a solid hydrogel post-UV exposure. Figures 26 and 27 highlight the change in structure of 10wt% F68 hydrogel. The Cellesi group method of functionalizing Pluronic F127 was successful in producing cross linked networks in the broader Pluronic library, amine terminated triblock copolymers such as Jeffamine ED 2003, and multiblock copolymers such as Tetronics (BASF trade name).

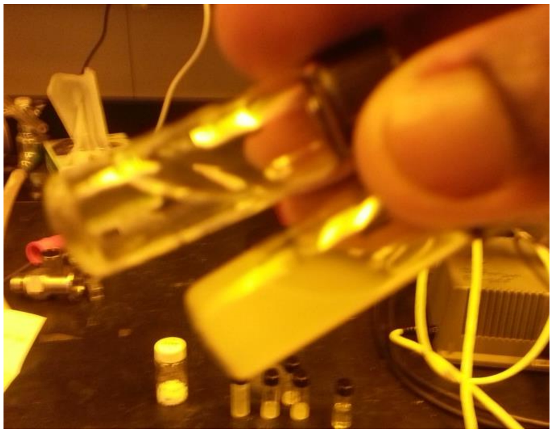

Figure 26. Before exposure to UV of 10 wt% F68DA (top) and 10wt% Jeffamine ED 2003DA (bottom).

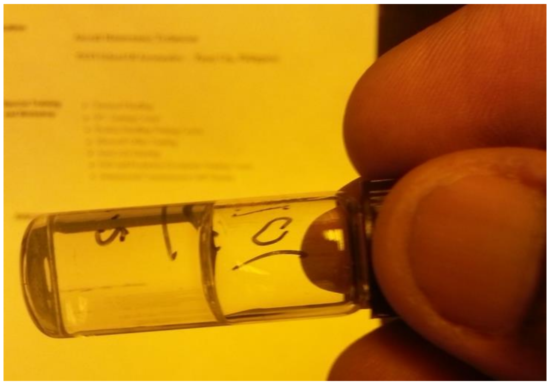

Figure 27. Solid, robust 10wt% F68 hydrogel post exposure to UV light.

In summary, a MW weight constraint was discovered for forming networks, and higher EO to PO ratio aided the free radical polymerization. Low MW PEG polymers cure well but are not of interest as scaffolding materials due to toxicity. Acrylate end groups proved to be sufficient for forming robust polymer networks for several PEO-PPO-PEO triblock copolymers including a large subset of the Pluronic and Tetronic libraries. Curing prevents shear-thinning behavior, so the material must be able to retain its shape for a short period of time post-extrusion. The next steps in this project are to quantify the change in viscosity of each polymer, to understand which materials have low yield strengths, and thus tailor the properties to form a desirable ink for 3D printing tissue scaffolds.

5.2 Yield Strength Evaluation

It was found that hydrogels like F127DA did not possess a robust enough structure post-extrusion for tissue scaffolds, so other hydrogels that would cure upon extrusion to form self-supporting structures were tested.

5.2.1 Organic Wax Rheology

Fugitive OW was used to explore the relationship between rheological results and printing behavior. Petroleum jelly is used as the solvent material while paraffin wax is the solute that is used as an additive to increase the G' of the overall material, thus the G' can be varied with paraffin wax and correlated with a printable material. Figure 28 shows the results of a steady state flow test and reveal that petroleum jelly has shear-thinning properties which make it an ideal modeling material for a 3DP ink.

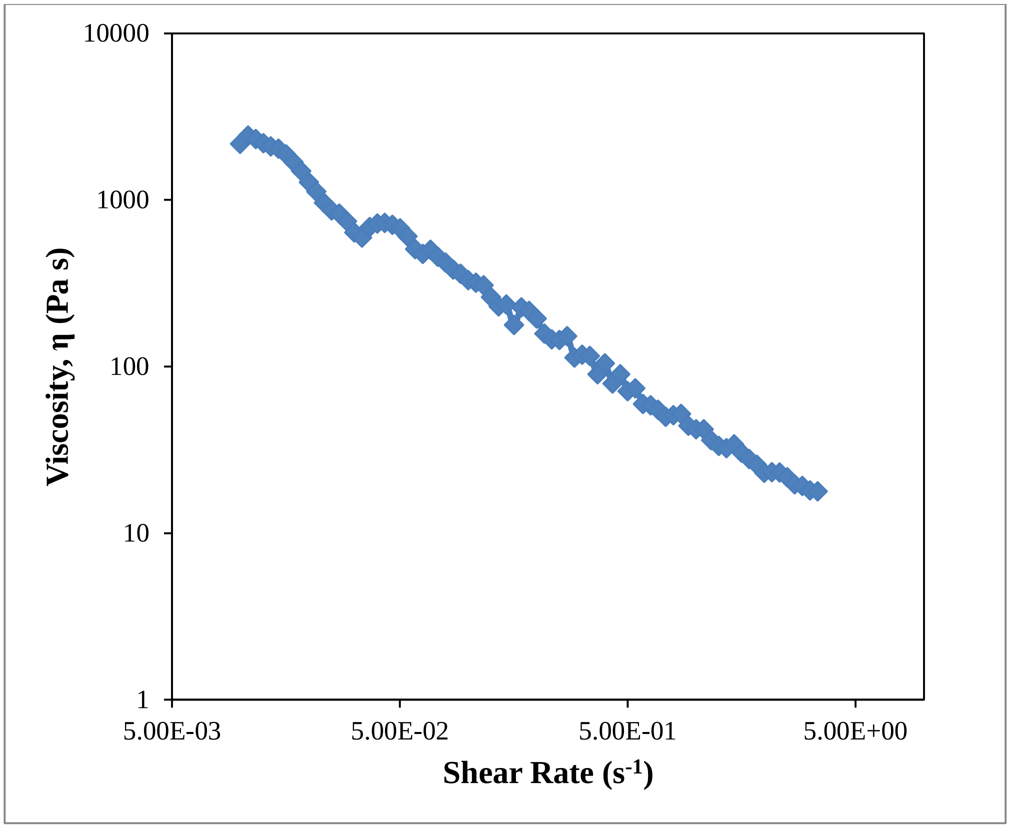

Figure 28. Steady state flow results of petroleum jelly show that this material is shear-thinning.

The yield stress was tested using oscillation stress sweeps from 0.1 up to 10,000Pa. The OW was prepared with a range from zero percent paraffin wax to 60 percent paraffin wax. Extrusion was possible from zero percent until slightly above 40wt% paraffin wax where the ink no longer printed below 90psi. Thus, the target range of study was from 0- 40wt%. The results of oscillation shear testing for the target range can be seen in Figure 29. There was a clear trend of increasing stiffness with increasing concentration of paraffin wax. The G' plateau was similar results published by Therriault et al. where they found a G' plateau around 10^6 Pa for 40wt% [16].

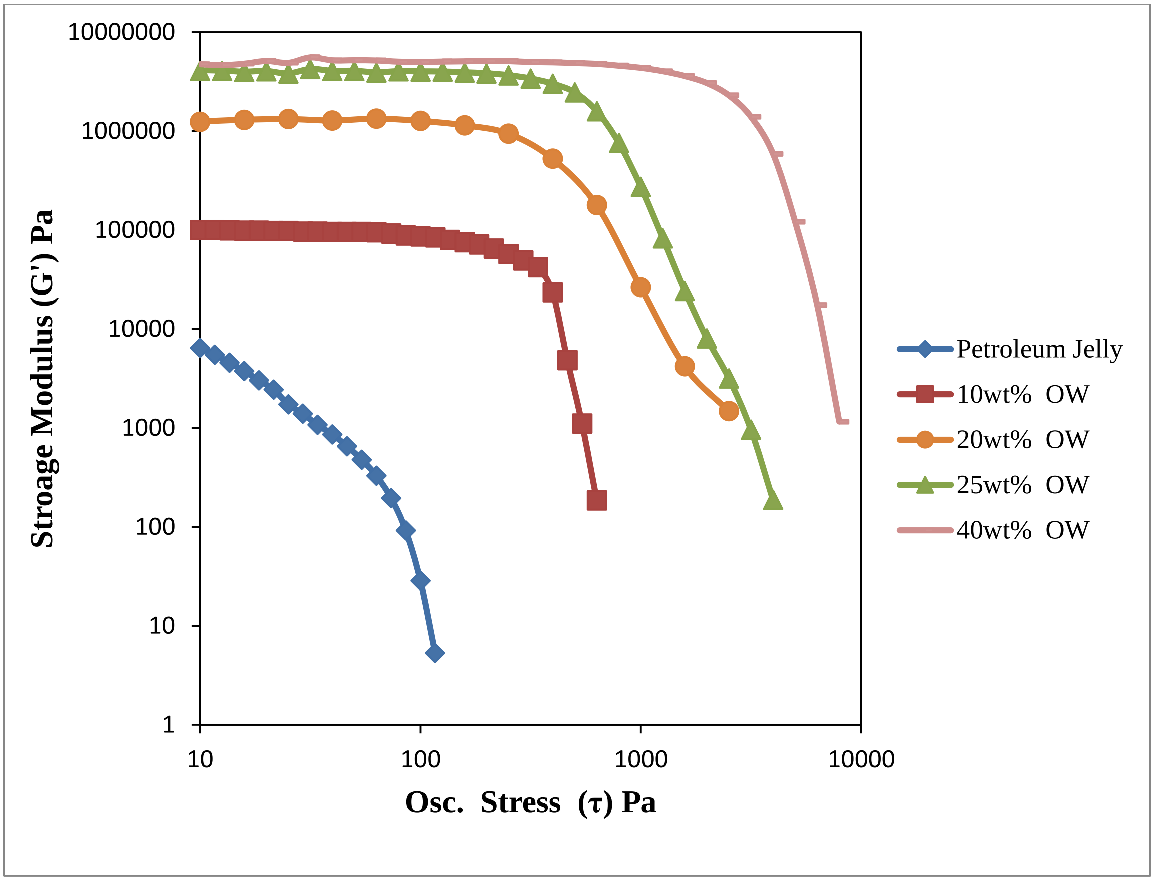

Figure 29. Increase of storage modulus with increasing weight percent of paraffin wax.

The critically applied yield stress was reported to be approximately 0.1G' or when the G' = G". The yield stress occurs at the fluid transition point which is also called the G', G" crossover point where the material yields and begins to flow. Due to the imprecise nature of yielding, the yield stress is commonly approximated based on a few methods. One method treats the plateau and the tail of the G' graph as two separate functions and approximates the value based on the intersection of two separate linear fits. This method is known as the lower limit to yield stress by Houwink [20]. A second method treats the yield stress to be the transition between the linear portion of G' to the tail. This is known as the upper yield stress, and is often estimated based on the G' plot. The lower and upper limits establish an area called the yield zone when yielding begins and continues until there is a noticeable flow. The final method discussed finds the yield stress as the peak in the stress-strain curve. This method reliably produces a yield stress that avoids approximations. The results of each method are shown in Figure 30. The 90% drop in G' seems to be an outlier when compared the other 3 methods. Since the stress-strain method falls within the yield zone, and produces an exact value, the yield stress will be reported according to this method.

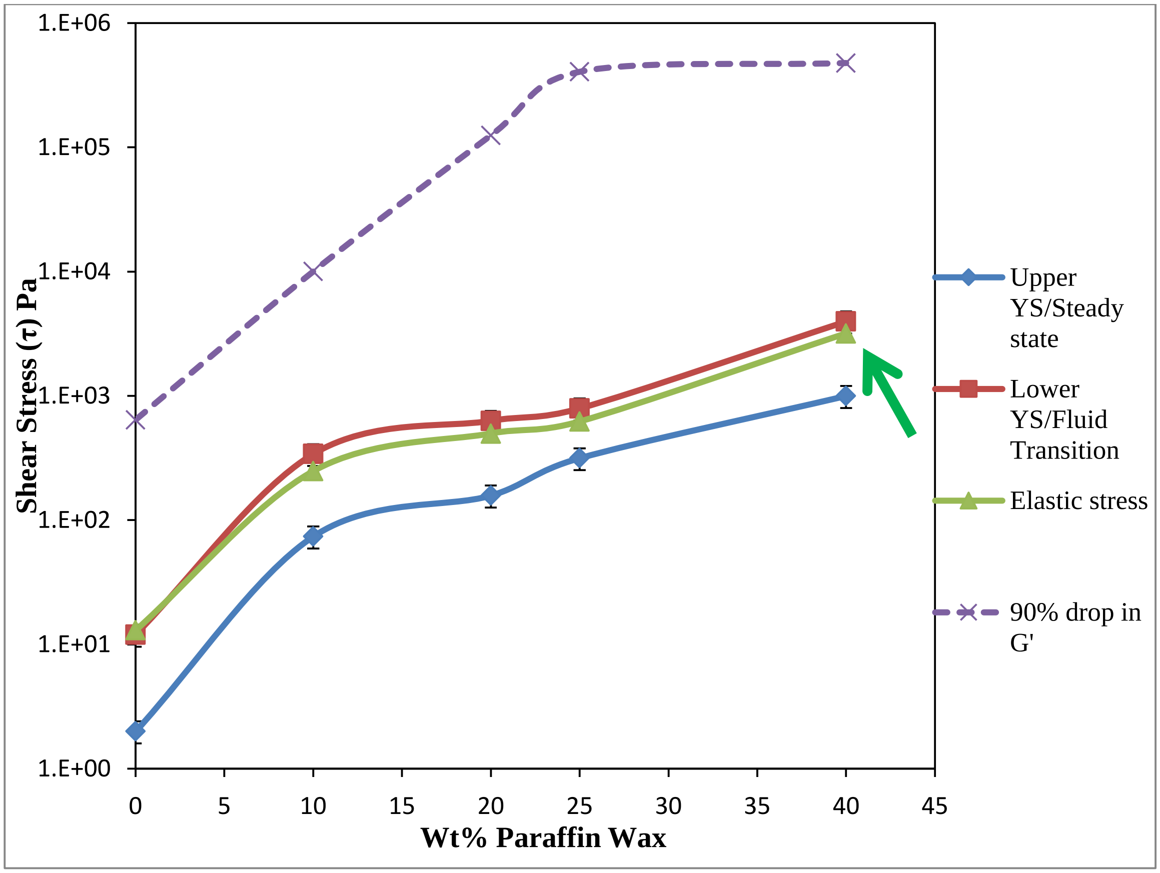

Figure 30. Comparison of different yield stress measurements.

5.2.2 Printing results Using Organic Wax

The next step to further understanding the correlation between rheological results and printing behavior was to print with the target materials. The nozzle diameter, write speed and pressure, and filament produced can be seen in Table 9. The write speed and pressure were chosen by what produced filaments with a diameter most similar to the diameter of the syringe tip used. Upon printing there was a noticeable difference between the pressure needed to start flow and the pressure need to sustain flow. In attempt to minimize the effect of time-dependent deformation, all printing results were reported after allowing the material to flow for 30s. Stiffer materials were printed using larger nozzle sizes, slower speeds, and higher pressures to achieve similar filament to nozzle diameter. Petroleum jelly and 10wt% paraffin wax spread post-extrusion, and 40wt% paraffin wax nearly clogged the printer. The ideal range was 20 to 25wt% paraffin wax.

Table 9. Printing results of OW ink.

	Petroleum Jelly	10wt% Paraffin	25 wt% Paraffin	40wt% Paraffin
Nozzle [µm]	250 	250	510 	510
Write speed [µm/s]	100	300	40	100
Pressure [psi]	Start: 5 Continue: 1.5	Start: 10 Continue: 4	Start: 50 Continue: 25	Start: 70 Continue: 30
Result	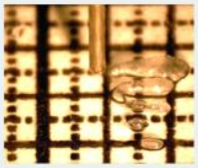	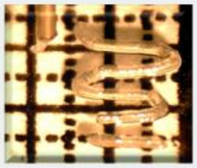	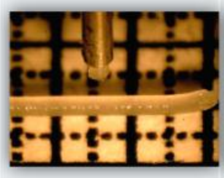	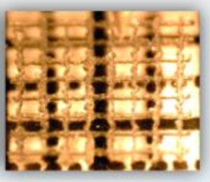

5.2.3 Correlating Rheology Results to Printing Behavior

Figure 31 shows the summary of yield strength that perform well with the DIW printing set-up. Below the target range, the extruded filaments spread into amorphous shapes, and above the target range, there was uneven printing behavior due to clogging. In conclusion, the OW wax studies identified a reliable method to measure yield stress using elastic stress to generate a stress strain curve, and identified the nozzle size, extrusion speed, and extrusion pressure needed to print filaments with a diameter similar to the nozzle diameter. The next experiments applied these results to the Pluronic inventory.

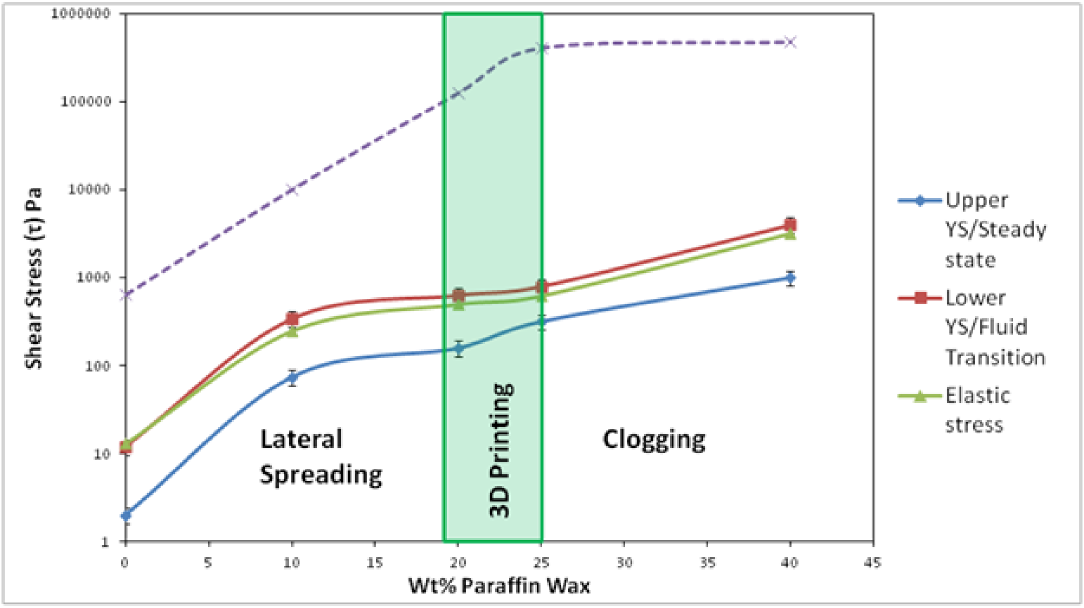

Figure 31. Comparison of different yield stress measurements.

5.3 Waxy Scaffolding Inks

A higher G' correlates to a material retaining its structure post-extrusion which is desirable for a printing ink. The Pluronic inventory includes several materials that are labeled starting with a P for paste. There are other structures with similar structures that form pastes such as Jeffamine ED 2003. Several pastes were evaluated for use as 3DP inks.

5.3.1 Selection Based on Stiffness and Yield Strength

Figure 32 displays the G' of possible starting materials with the last material being Pluronic L121 which is a liquid as a point of comparison. A 23wt% F127 hydrogel was also included as a reference to show that the pastes range from softer than petroleum jelly to hard waxes. Liquids tested generally had a G' of less than one Pa. The green box shows the range of G' values that were determined to correlate to ease of printing and retention of shape post-extrusion based on the OW studies. Pluronics P85 and P105 and

Jeffamine ED 2003 fell within the desirable range. Table 10 shows that only two polymers can be printed neatly without plasticizers: P103 and P123. This mostly is due to the materials having a higher yield stress at the G' values than the OW. Both P103 and P123 also spread laterally post-extrusion making them unsuitable candidates as inks. Applying a similar logic learned from the OW studies, the next step in the design process was to formulate an ink and mix a plasticizer into a stiffer polymer paste to tailor the properties to print as summarized by Figure 33. Table 10 displays a summarized list of the tested formulations, and each mixture was made according to the process in Figure 21. The most successful of the group was a 70wt% mixture of P85DA with 25wt% L121 and 5wt% photoinitiator. The yield stress of this formulation had a local maxima at 585Pa which was within the range of yield stress values of the 20 and 25wt% OW formulations as seen in Figure 34.

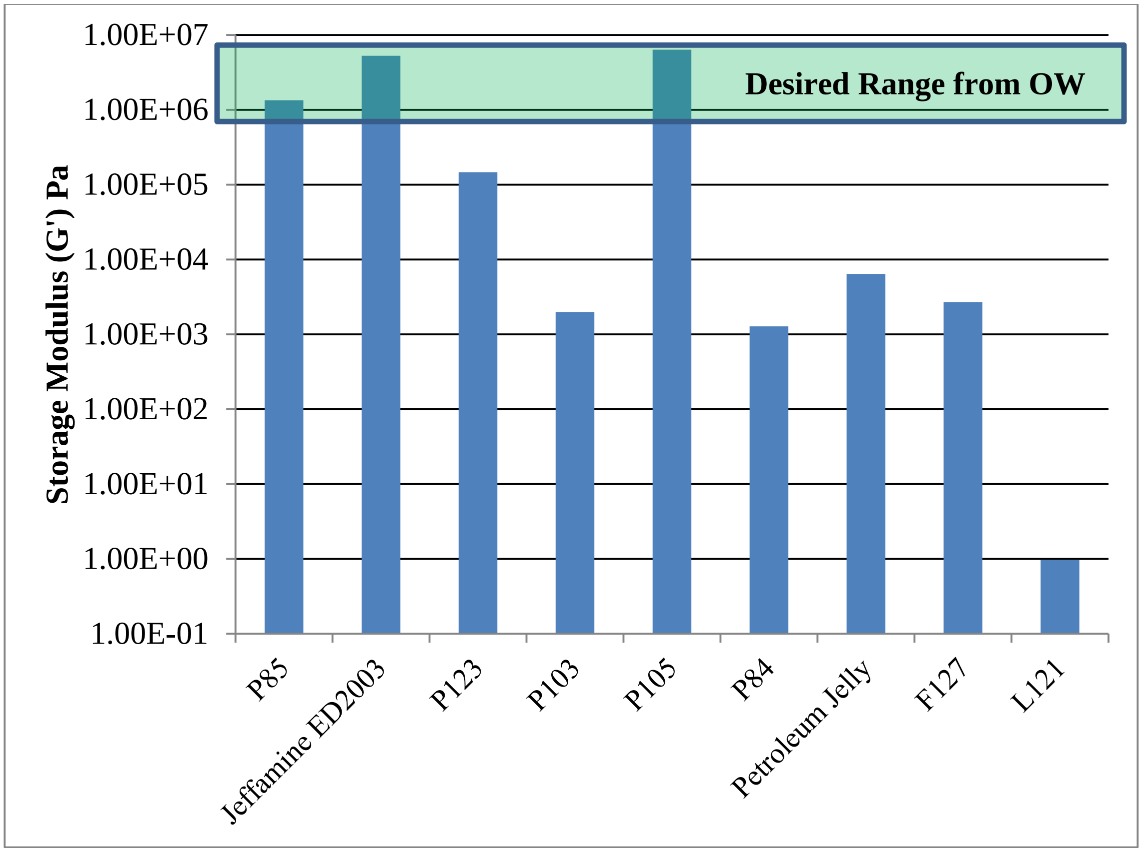

Figure 32. Summary of G' values of the paste inventory. The green box is the range correlated to desired printing behavior based on results from the OW studies. Pluronic F127 and L121 where included as reference points.

Table 10.   Results of printing neat polymers

Pluronic	MW	prints	η* [Pa•s]	Smallest syringe tip [µm]	Lowest Write Pressure [psi]
P85	4600	Too Solid	5.00E+05	NA	NA
Jeffamine ED2003	2000	Too Solid	9.00E+05	NA	NA
P123	5750	**Yes**	2.45E+03	254	85
P103	4950	**Yes**	3.42E+02	50	40
P105	6500	Too Solid	1.00E+06	NA	NA
L121	4400	Too Liquid	9.76E-01	NA	NA
F127	12200	Yes - 23wt% hydrogel	2.71E+03	NA	NA
L64	2900	Too Liquid	8.20E-01	NA	NA
1301	6800	Too Liquid	1.60E+00	NA	NA
90R4	7240	Too Liquid	2.90E+00	NA	NA

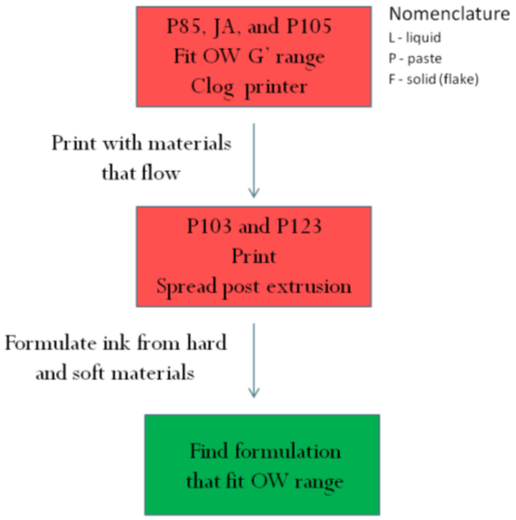

Figure 33.   Flow of choice to use paste ink formulation rather than pure Pluronic pastes.

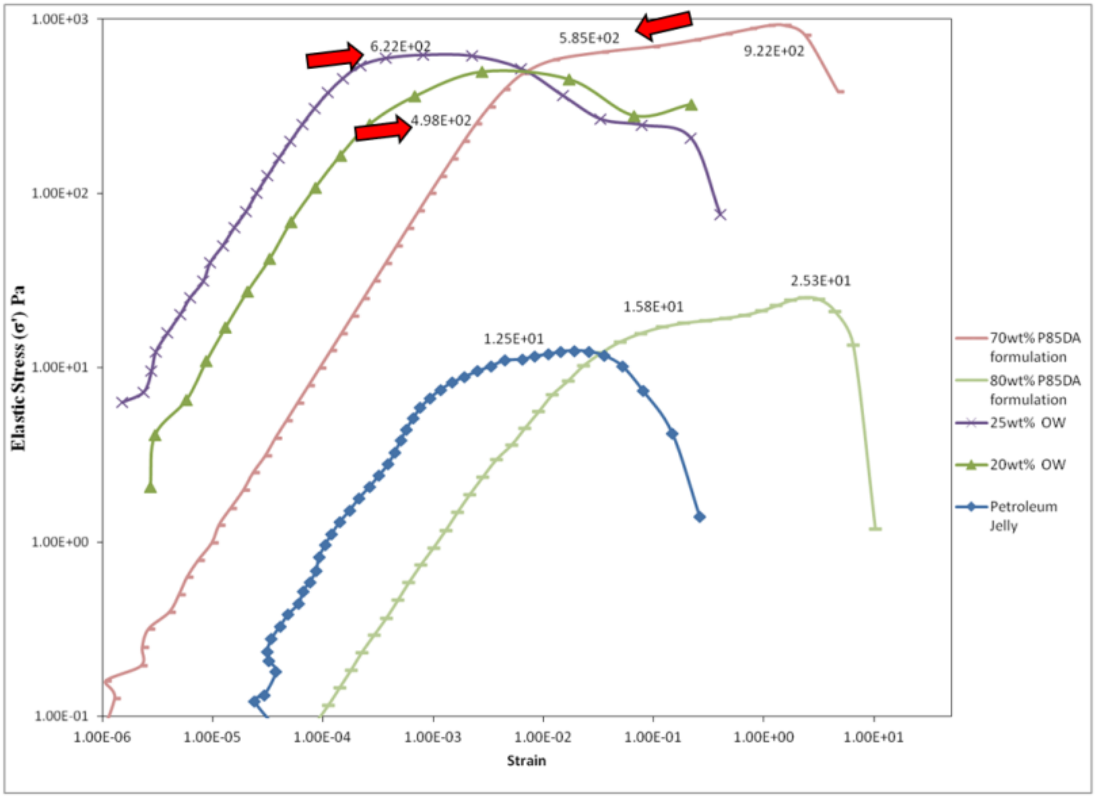

Figure 34. Choice of ink formulation based on printing results and correlation to OW rheology.

5.3.3 Printing Results

Although other inks produced successful results in various areas, this section highlights the printing achievements and scaffolding structures fabricated using primarily the 70wt% P85DA formulation, which was the most successful 3DP ink material. The 70wt% P85DA formulation was capable of being printed at a higher resolution than the OW at higher speeds with better control. The smallest nozzle diameter that could be printed was 50μm, but the printing behavior was much more consistent with a 100μm syringe. To avoid creep studies on this material, 60psi was found to cause near instantaneous yet even flow. The results in Table 11 show that although 60wt% flows and retains its shape, 70wt% demonstrates better superior scaffolding results.

Table 11. Summary of printing results for most successful P85DA ink formulations

	60wt% P85DA	70wt% P85DA
Write speed [µm/s]	200 	150 
Nozzle [µm]	260	100
Pressure [psi]	40	60
Result	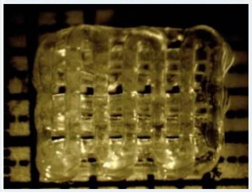	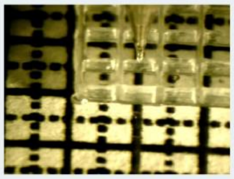

The 70wt% P85DA formulation was also successful for printing more complex shapes. The first complex shape was a 5000μm pillar as seen in Figure 35. Pillars are useful to establish the potential for excellent layer resolution, self-supported structures, and controlled printing. Figure 35a shows a small drop was extruded as the base for the pillar was needed. The pillar was 30:1 height to width, and was cured post-extrusion. Figure 35 b shows the final product; every printed pillar was flexible, yet resumed its original shape after being crushed, bent, and stretched. Subsequently more complex structures were attempted. A 1cubic cm scaffold was printed by depositing over 100 layers as seen in Figure 36. This structure was cured in situ to aid the layer separation. After printing bigger structures, the resolution of the DIW printer was evaluated by printing scaffolds with decreasing area as seen in Figure 37. Controllable structures were printed until 0.25mm^2. At 0.25mm^2 lateral spreading begins to occur, and the well size is not the same as CAD model. When printing 0.1mm^2 there is enough spreading to cause irregular well shapes. A remaining test was to soak the material in THF to evaluate the degradation of the acrylate groups. Figure 38 shows two identically printed structures. The top row was printed using P85DA and the bottom row was printed using just P85. Upon exposure to UV light, the diacrylate functionalized ink becomes more opaque and the un-endcapped ink remains the same. After being soaked in THF for 10 minutes, the cross-linked ink curled from absorbing THF while the un-endcapped ink completely dissolved.

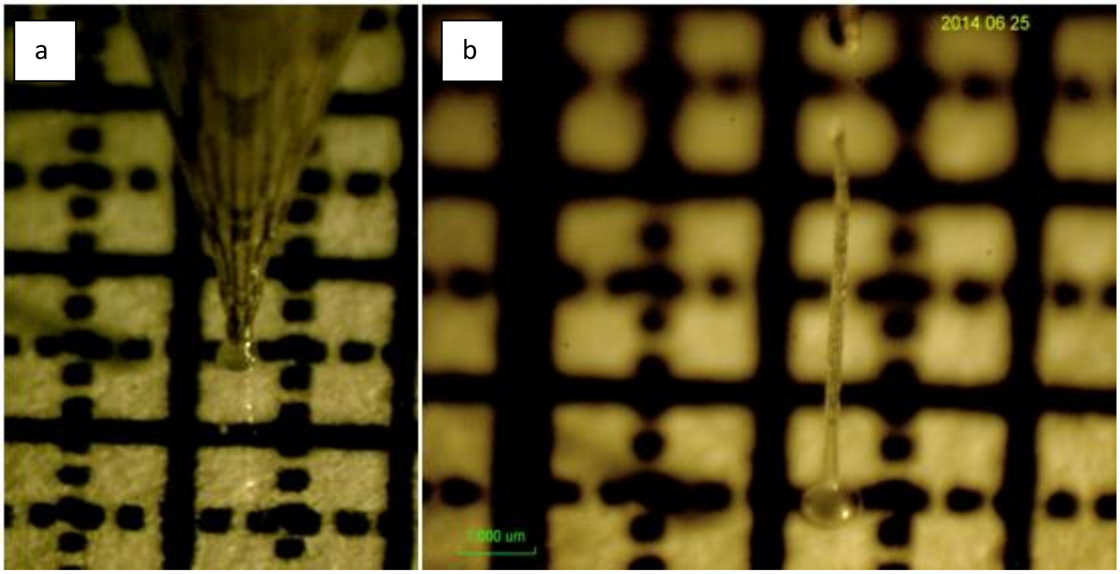

Figure 35. Printing 3000 μm tall pillar us 70wt% P85DA formulation. a) is the printing of a small base and b) the final cured pillar.

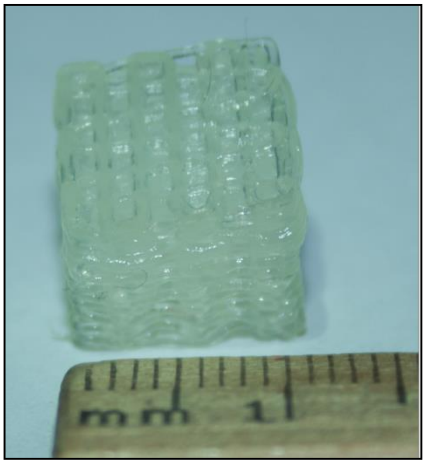

Figure 36. Larger $1cm^3$ scaffold printed using P85DA.

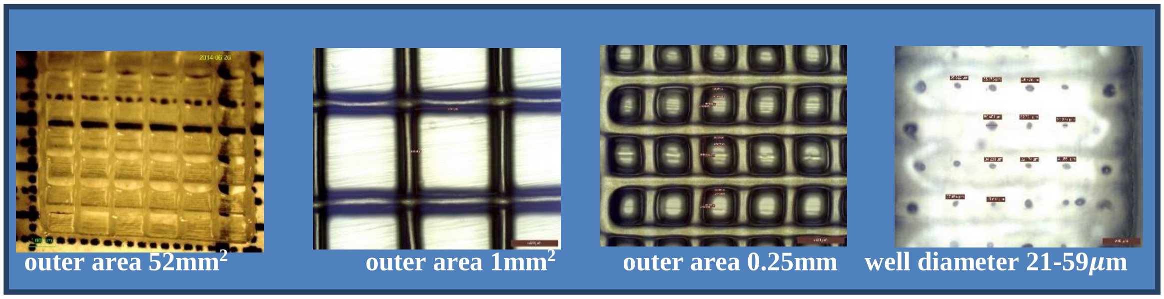

Figure 37. Challenges with size reduction is that the overall resolution decreases.

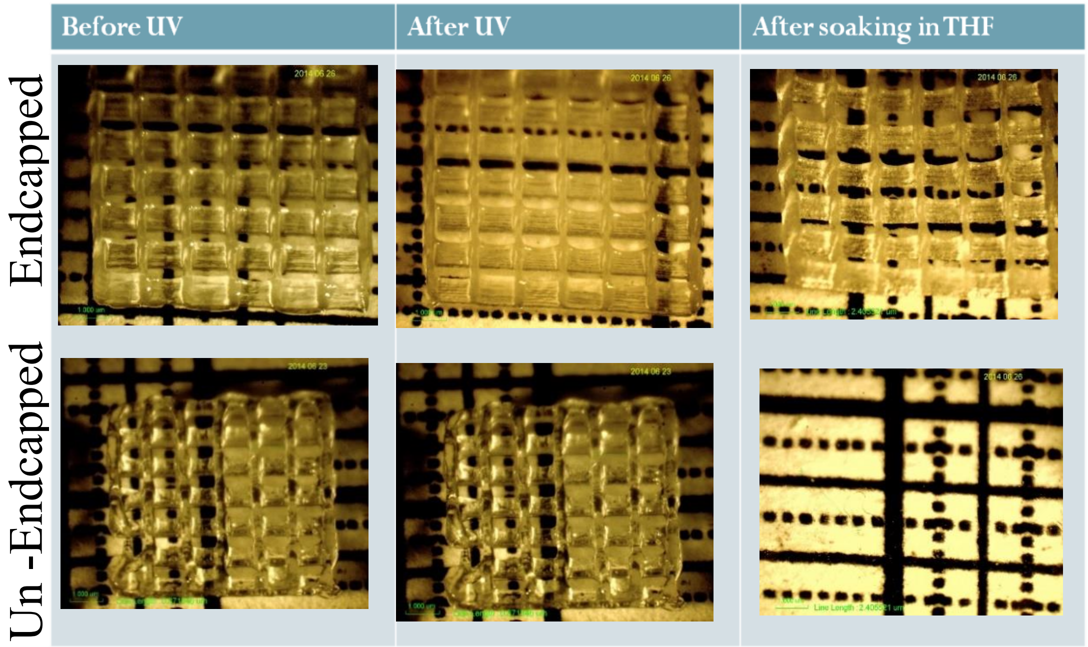

Figure 38. Test of degradation of cross-linked polymer network of 70wt% P85DA formulation.

In summary, waxy polymer starting materials are suitable for fabricating complex scaffolds. Specifically, a 70wt% formulation with 25wt% L121DA and 5wt% photoinitiator was the best printing material out of all tried materials in Table 7.

5.4 Swelling Behavior of Pluronic P85DA Formulation

The percent swelling is a straightforward indicator of biocompatibility. The polymer scaffold should be able to absorb and hold nutrients to sustain cell growth. A 16 layer grid constructed from 70wt% P85DA, 25wt% L121DA, and 5wt% photoinitiator was submerged in de-ionized, ultrapure water for 150 days. The percent swelling can be seen in Figure 39. Within one day the scaffold absorbed 1.6 times its weight in water and eventually reached a saturation point of 1.8 times its original weight. Pollock et al. found that a 20wt% F127 hydrogel absorbs 2.5 times its original weight after five hours [33].

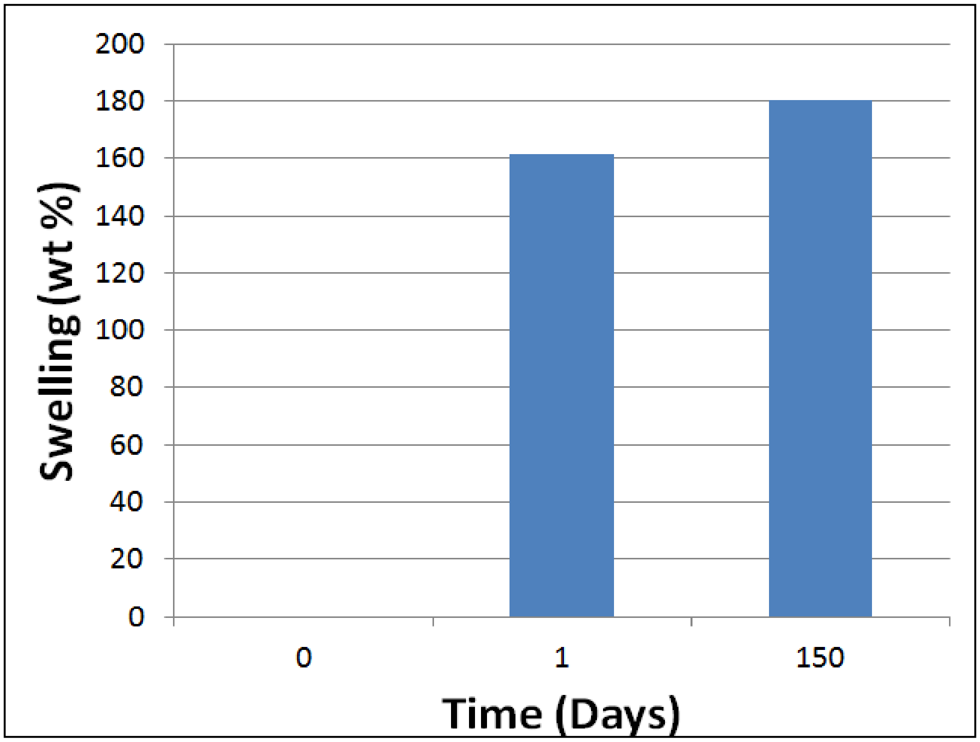

Figure 39. Swelling of 70 wt% P85 with L121 formulation in milliQ water.

5.5 Mechanical and Thermogravimetric Results

The field of TE incorporates many materials engineering problems and requires novel materials with specific strengths for unique applications. Currently a class of materials called hydrogels are popularly used, but hydrogels are limited by their poor mechanical strength. The Lewis group at Harvard has developed biomimetic systems using Pluronic F-127, extra cellular matrices for neural cell cultures using poly (2-

hydroxyethyl methacrylate) (p-HEMA), and scaffolds for bone cultures using silk/Hydroxyapatite (HA) filaments. Each of these materials are biocompatible and have characteristics that are conducive to growing specific types of cells. UV curing is used to increase the mechanical strength of these materials. The challenge when printing a scaffold is to have a material that shear thins and flows through a syringe tip under air pressure, but hardens upon extrusion and retains its shape long enough to be cured.

The two variables of this experiment will be cure time and concentration of the photoinitiator, Durocur 1173. Two sets of data were gathered from the tensile tester for a set concentration of photoinitiator and varying cure time. The other set of data is for a set cure time and varying concentration of photoinitiator.

5.5.1 Tensile Testing

The Pluronic specimens were very soft which made them difficult to test as they were crushed in the Instron grips. This made many samples fracture at the tab instead of the gauge length. A quick set epoxy as presented in Figure 40 was used to encase both ends of the specimens in a hardened layer to protect the tabs. Figure 41 shows the position where the epoxy was applied on the specimens.

Figure 40. Quick set epoxy used to generate hard outer casings for the tabs at both ends of the Pluronic P85 specimens.

Figure 41. Location where epoxy was used to reinforce the tabs at the ends of the dogbone sample.

Stress versus strain curves for pluronic specimens are presented in Figures 42 through 44. The ultimate tensile strength is 190 kPa for the 10 wt% photoinitiator sample, 160 kPa for the 5wt% photoinitiator sample, and 260 kPa for the 1 wt% photoinitiator sample. The ultimate tensile strength versus wt% photoinitiator is presented in Figure 45. It shows that 1wt% photoinitiator sample has the highest ultimate tensile strength while the 5wt% photoinitiator has the lowest ultimate tensile strength.

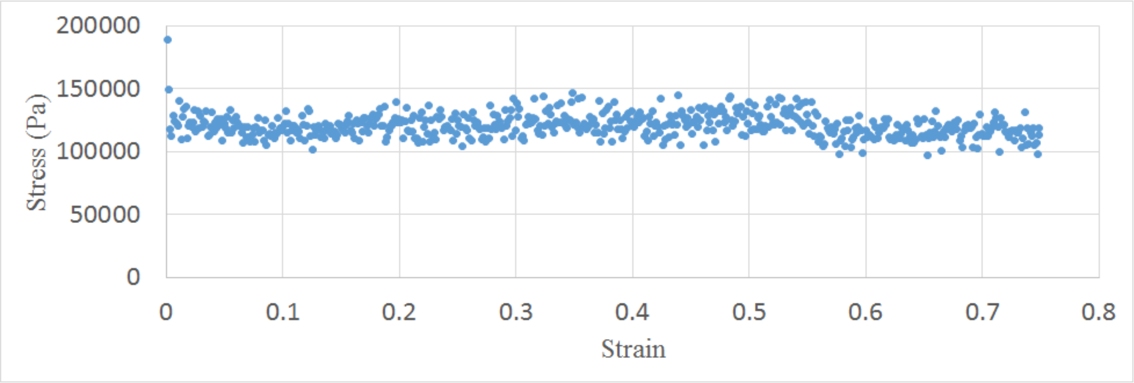

Figure 42. Stress vs strain for pluronic P85 samples with photoinitiator concentration of 10 wt%.

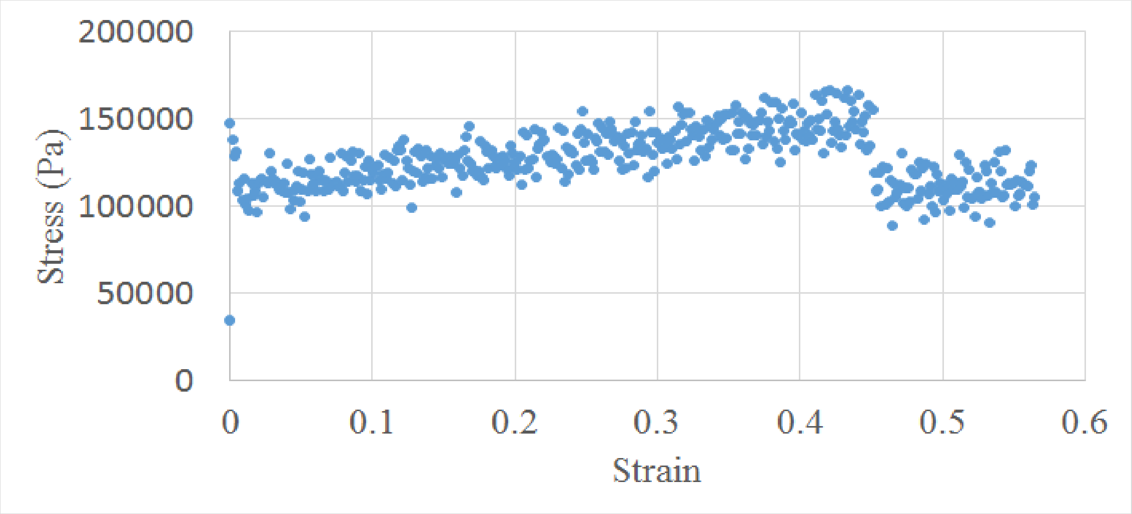

Figure 43. Stress vs strain for pluronic P85 samples with photoinitiator concentration of 5 wt%.

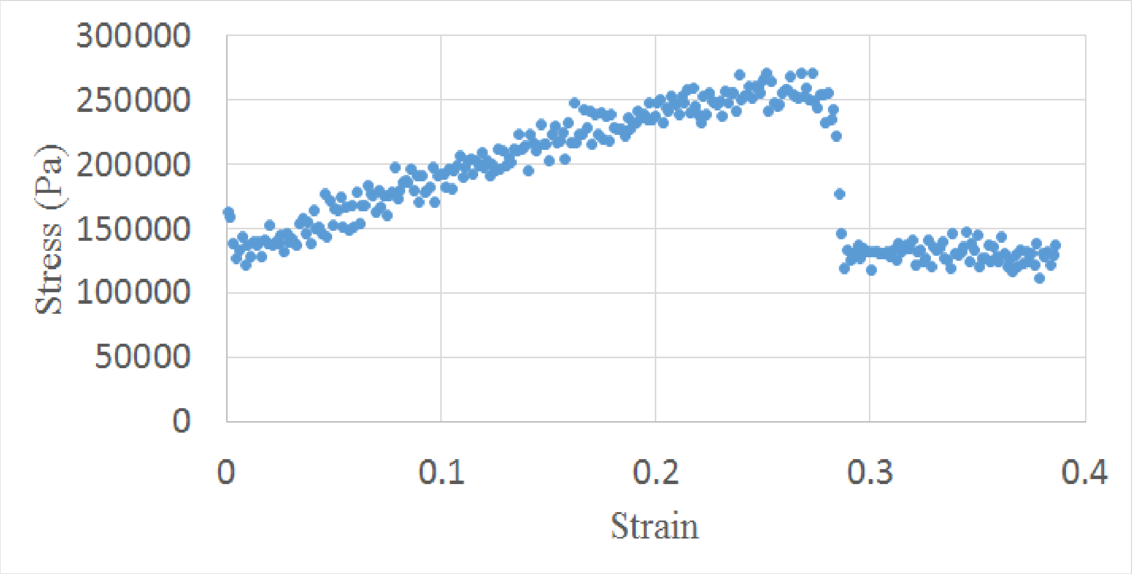

Figure 44. Stress vs strain for pluronic P85 samples with photoinitiator concentration of 1 wt%.

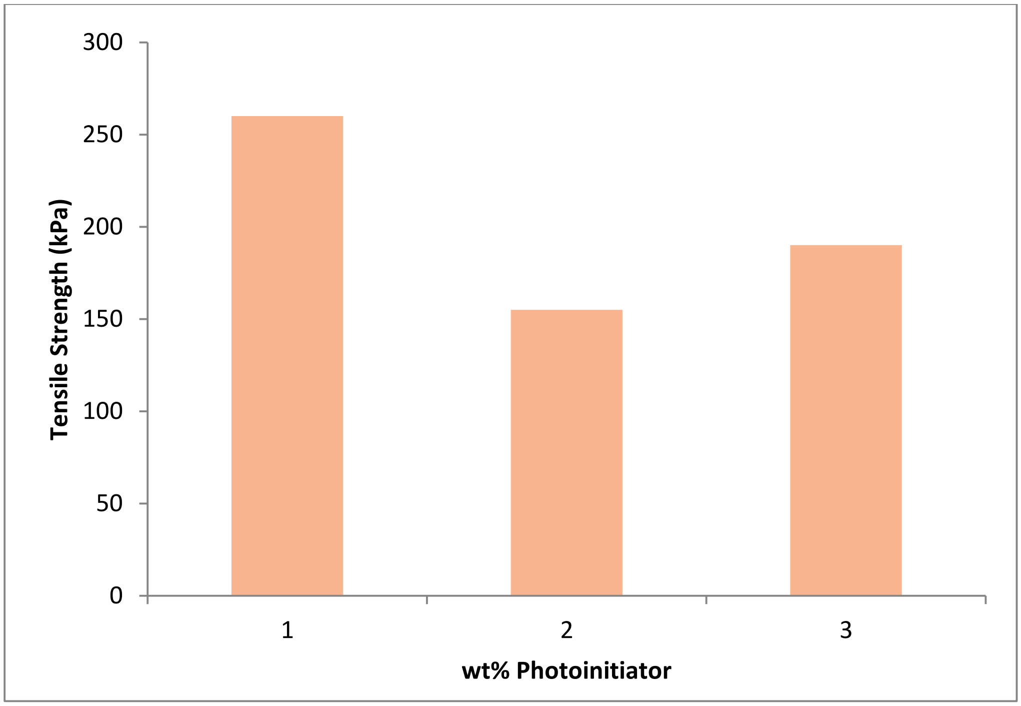

Figure 45. Tensile strength versus wt% photoinitiator for three pluronic P85 samples.

Percent elongation at fracture versus wt% photoinitiator for the pluronic P85 samples is presented in Figure 46. The percent elongation at fracture increases linearly with respect to the weight percent photoinitiator shown by the R_squared value of 0.99. The 10wt% photoinitiator sample has the highest percent elongation at fracture, and the 1wt% photoinitiator sample has the lowest percent elongation at fracture.

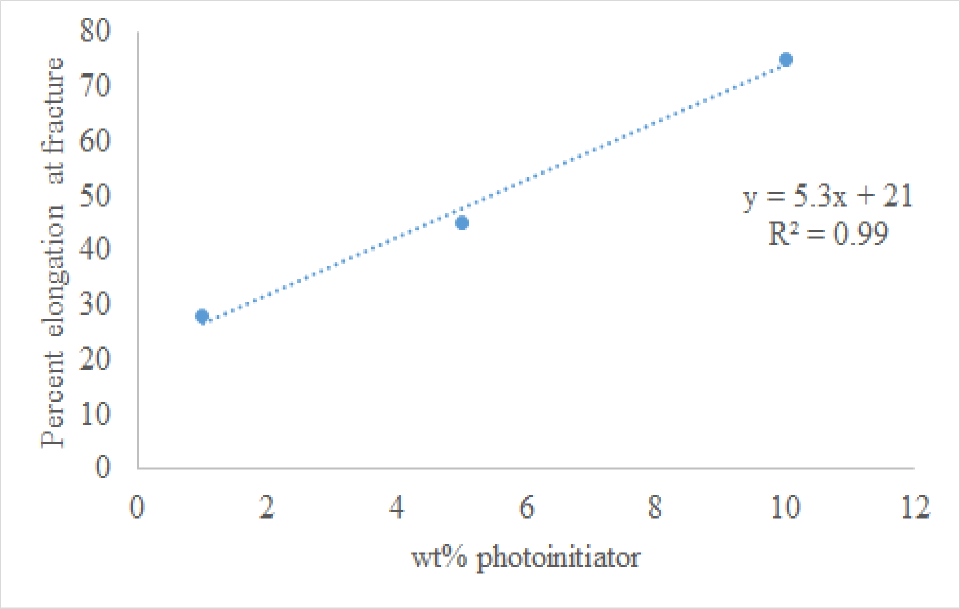

Figure 46. Percent elongation at fracture vs. wt% photoinitiator for three pluronic P85 samples.

Only three of the eight tensile specimens were able to generate useful data as the material tended to tear at the grips. The data in the elastic region for these three specimens are missing in Figure 42 through Figure 44. This is due to the use of a 50 kN load cell used in the experiment which can only measure the values down to 100 N [13]. The 50kN load cell was used due to lack of access to grips that fit the smaller load cells. This introduces considerable error in the tensile data so the tensile strengths should only be used as a comparison between the specimens and should not be viewed as correct strength values. As shown in Figure 45, the highest measured tensile strength occurred when the photoinitiator concentration was 1 wt%. This was similar to results found in literature for vinyl ester and epoxy. Figure 47 shows that the vinyl ester and epoxy samples also reached their highest tensile strength at 1 wt% photoinitiator. A larger concentration of photoinitiator in the process can weaken the bonds between polymers because photoinitiator generates free radicals to initiate the curing process [40]. This generates faster polymerization rates which generate smaller polymer chains, decreasing the strength of the material due to lower crystallinity.

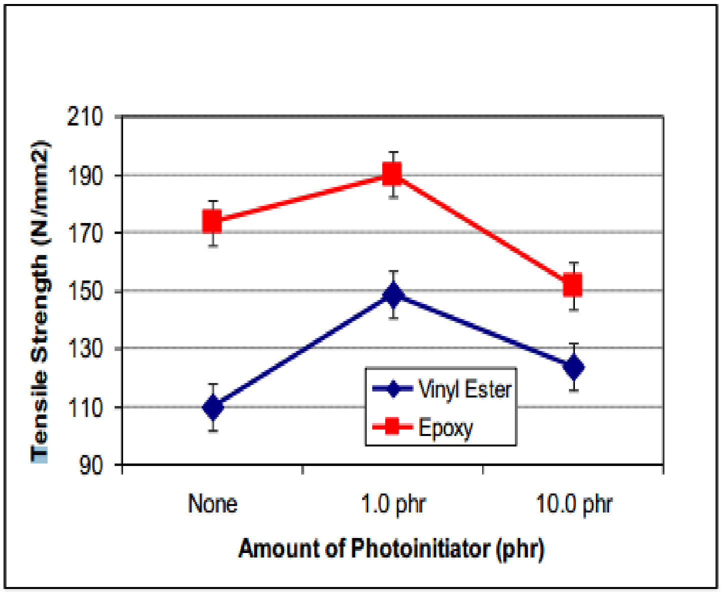

Figure 47. Tensile strength versus amount of photoinitiator of vinyl ester and epoxy [40].

The percent elongation at fracture increases linearly with respect to the weight percent photoinitiator as shown in Figure 46. This shows that the presence of photoinitiator affects the percent elongation at fracture of the Pluronic specimens. As previously discussed, this is likely due to smaller chain lengths occurring from a greater polymerization rate.

The accuracy of the tensile tests could not be confirmed because the elastic region was missing from the stress versus strain curve presented in Figure 42 through 44. Without the elastic region, the Young’s modulus could not be calculated and compared to literature values. However, since an extensometer was not used during this experiment, the elastic modulus likely would not have matched literature values. Due to not using an extensometer, the percent elongation data shown in Figure 46 should only be used as a comparison between the tested samples to show the general trend of how concentration of photoinitiator affected the polymer.

5.5.2 Dynamic Mechanical Analysis

Viscoelastic properties of the Pluronic F85 specimens were tested using Dynamic Mechanical Analysis (DMA). Three specimens were examined. These specimens had a cure time of 60 min and varying percent photoinitiator added to the formulation. The instrument was a TA Instruments DMA 2980.

DMA is very sensitive to transitions, particularly the glass transition temperature Tg. The calculation of Tg followed ASTM D4065. The mechanical properties degrade drastically at the Tg. At the Tg, there is a large decrease in the storage modulus and a concurrent peak in the tan delta.

Figure 48 shows an overlay for the storage modulus and the tan delta plots. This graph is for the sample with 0.1 wt% photoinitiator. The two other samples display the same features, including abrupt decreases in the storage modulus plot and the peak in the tan delta plot corresponding to Tg. For the tan delta plot, all samples also showed a constant region (glassy regime) preceding the Tg peak. Figure 49 shows the tan delta of this glassy regime versus the wt% photoinitiator. All values for tan delta were less than 0.30. For the three samples, the storage modulus in the glassy regime ranged from 20 to 55 MPa.

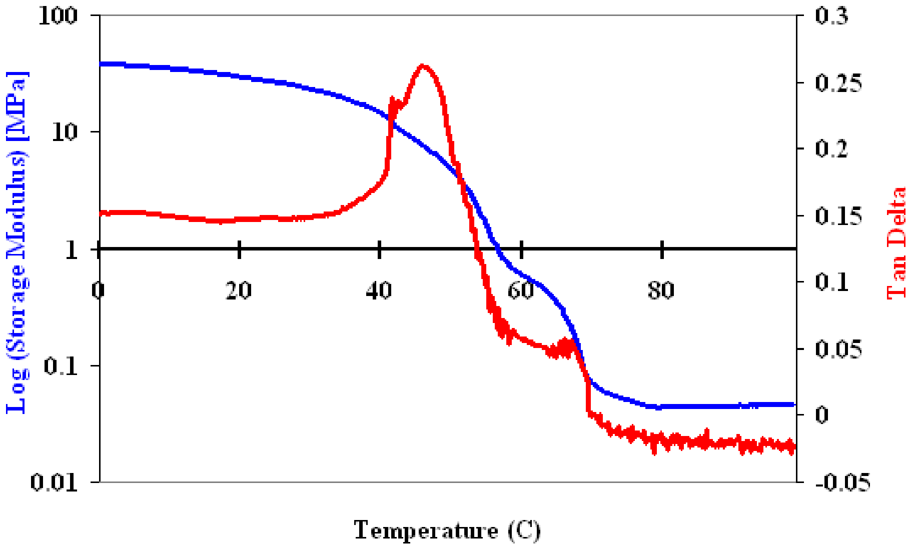

Figure 48. Overlay for the storage modulus and the tan delta for the sample with 0.1% wt photoinitiator.

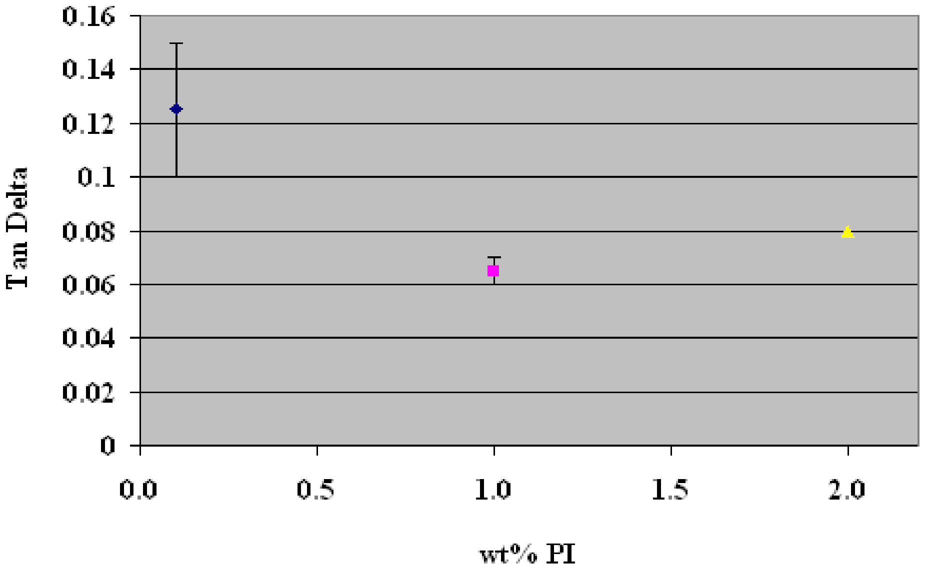

Figure 49. Tan delta of glassy regime vs. wt% photoinitiator for three DMA specimens.

Figure 50 shows the glass transition temperature Tg versus wt% photoinitiator. The data points represent the mean values from two heating cycles for each specimen. The error bars represent the calculated uncertainty in these values.

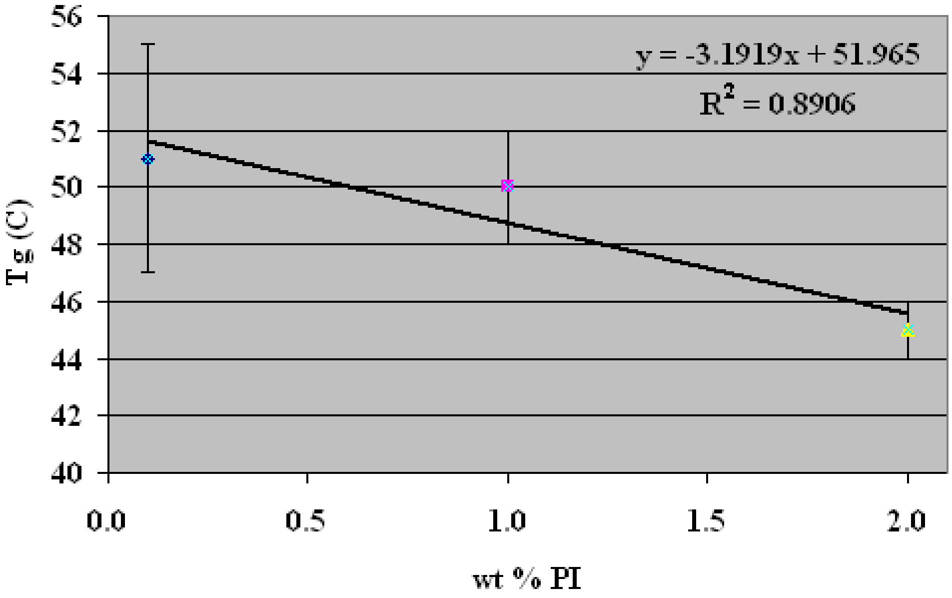

Figure 50. Glass transition temperature Tg vs wt% photoinitiator for three DMA specimens.

Figure 49 showed that the tan delta values are below 0.30 for each specimen, which means that the specimens are more elastic than viscous. Since tan delta is the ratio of G' to G", very viscous materials have a tan delta of greater than 1.00. Using tan delta values was a qualitative way to check the homogeneity of the curing process. All specimens were cured for 60 minutes, suggesting that this cure time was sufficient for synthesizing elastic specimens. For all three samples, the storage modulus in the glassy regime ranged from 20 to 55 MPa. This exceeded the value of 8 MPa for Young’s tensile modulus of polyhydroxyoctanoate, a very weak biopolymer used for TEengineering [41]. Although the storage modulus and Young’s modulus are not the same due to differing loading conditions, it was still promising that our Pluronic specimens exhibited a relatively large storage modulus.

Figure 50 showed a decrease in Tg with an increase in the weight percentage of photoinitiator. The linear regression line shown in Figure 50 did not fit the data very well, and a greater number of test samples would be necessary to model the relationship between Tg and photoinitiator concentration. Literature values ranged from 35 to 65C for polylactide and polyglycolide, similar biopolymer materials used for TE [41]. The measured Tg values from our experiment are reasonably within the range of the literature values. The uncertainties of the tan delta and Tg values followed the same trend as the uncertainty of the hardness values. That is, the uncertainty of the mean values decreased as the wt% of photoinitiator increased.

It was found that the addition of greater weight percent photoinitiator decreased the hardness, increased the elongation at failure, and decreased the glass transition temperature of the Pluronic specimens. All three tests, DMA, tensile testing and hardness testing showed that an increase in initiator concentration had a softening effect on the polymer. This was due to the generation of smaller chain lengths from the rapid polymerization that took place with greater initiator concentration. It was also found that an increase in cure time increased the hardness of the specimens, and the specimens were found to be very elastic in nature with tan delta values of less than 0.30 from DMA testing.

5.5.3 Thermal Gravimetric Analysis

The degradation of pure P85, P85DA, an uncured 70wt% P85DA formulation, and a cured 70wt% formulated were tested using TGA and DSC. The phase transitions were incomprehensible via DSC due to the mixture of two polymers and a photoinitiator; however TGA revealed one interesting peak that is discussed below. One milligram of each sample was heated in air over a wide temperature range of 25 - 600^{o}C at a slow pace of $2^{\circ}C/min$ to isolate any possible transitions. Pure P85 was analyzed to attain an understanding of the bulk behavior. The inflection point was found at the peak of the first derivative of the curve at 270^{o}C. The greatest loss of mass was due to the degradation of the ester linkages. Functionalizing P85 shifted the inflection point to 280^{o}C. The inflection points of the uncured and cured formulations were 160^{o}C and 340^{o}C. Figure 52 shows displays the results for each sample. Figure 52 d shows that the cured sample has one sharp peak at 340^{o}C which can be attributed to the specific temperature needed to break carbon-carbon bonds formed in the polymerization.

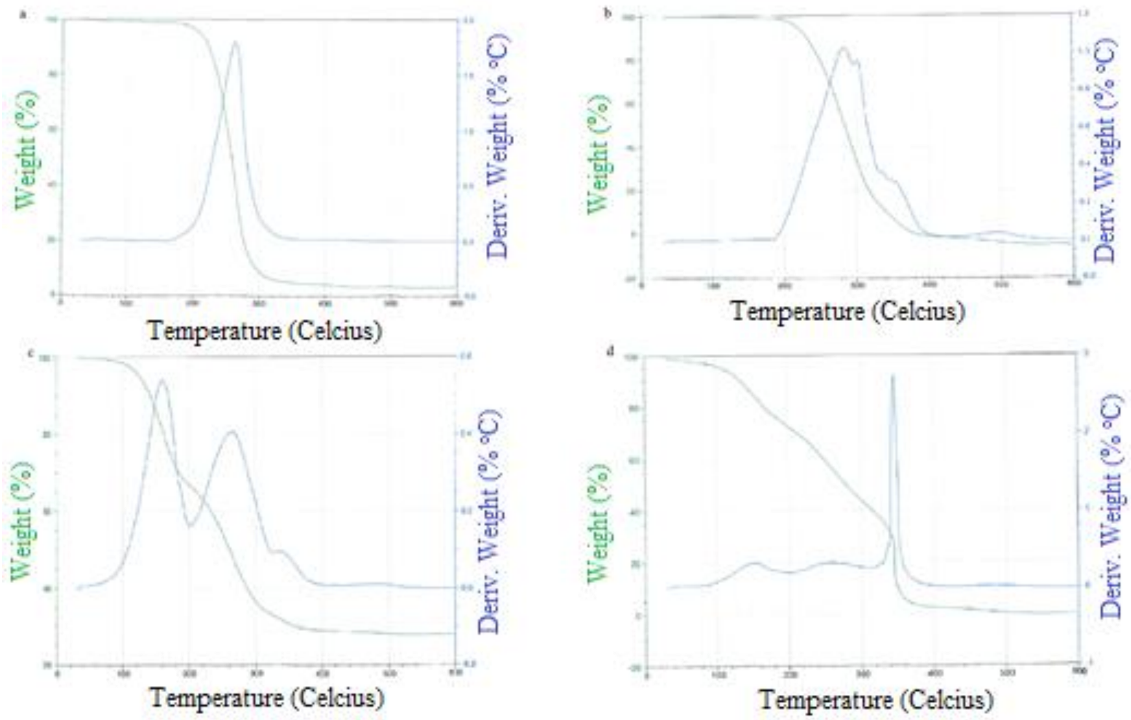

Figure 51. TGA results of a) P85, b) uncured P85DA, c) uncured 70wt% P85DA, 25wt% L121DA, and 5wt% Darocur 1173, and d) cured 70wt% P85DA, 25wt% L121DA, and 5wt% Darocur 1173.

CHAPTER SIX
CONCLUSIONS AND FUTURE WORK

As discussed in the literature review, wax materials have more broadly tunable properties with ranges in stiffness and yield strength that have the potential to outperform conventionally used materials such as Pluronic F127 and other hydrogels. Complex scaffolding structures such as pillars and woodpiles were successfully printed using commercially available wax starting materials, and the scale of the scaffolds varied from micron sized wells to large one centimeter length cubes. These data will help to identify new materials that more closely match the elasticity of tissues to synthesize better scaffolds. The stiffness, yield strength, and viscosities of wax and Pluronic paste based materials are highly tunable, easily controlled, and more versatile than liquid and solid Pluronics. Because of their controllable properties, paste-based inks are viable 3DP inks and should be considered for future studies.

Future work with this topic should include characterization of the polymerization mechanisms or 4arm materials such as the Tetronics library to aid resolution and cell viability studies of Pluronic P85, Jeffamine ED 2003, and other paste based inks. Also to continue this work, it could become necessary to quantify comparisons between rheology and printing behavior using fluid flow modeling software because rheological shearing differs from fluid flow through cylindrical and conical syringe barrels.

REFERENCES

1. R.A. Barry, R.F. Shepherd, J.N. Hanson, R.G. Nuzzo, P. Wiltzius and J.A. Lewis, *"Direct-Write assembly of 3D hydrogel scaffolds for guided cell growth,"* Advanced Materials, **21**, 2407-2410 (2009).

2. R.B. Bird, W.E. Stewart and E.N. Lightfoot, *"Transport phenomena. 2nd,"* Wiley, **604**, 605 (2002).

3. S. Bose, S. Vahabzadeh and A. Bandyopadhyay, *"Bone tissue engineering using 3D printing,"* Materials Today, **16**, 496-504 (2013).

4. F.P.W. Melchels, M.A.N. Domingos, T.J. Klein, J. Malda, P.J. Bartolo and D.W. Hutmacher, *"Additive manufacturing of tissues and organs,"* **37**, 1079-1104 (2012).

5. R. Lanza, R. Langer and J.P. Vacanti, Principles of Tissue Engineering (Academic press. 2011).

6. J.A. Lewis, *"Direct ink writing of 3D functional materials,"* Advanced Functional Materials, **16**, 2193-2204 (2006).

7. G.M. Whitesides, *"The origins and the future of microfluidics,"* Nature, **442**, 368-373 (2006).

8. D. Therriault, S.R. White and J.A. Lewis, *"Chaotic mixing in three-dimensional microvascular networks fabricated by direct-write assembly,"* Nature Materials, **2**, 265-271 (2003).

9. E.B. Duoss, M. Twardowski and J.A. Lewis, *"Sol-Gel inks for Direct-Write assembly of functional oxides,"* Advanced Materials, **19**, 3485-3489 (2007).

10. J.N. Hanson Shepherd, S.T. Parker, R.F. Shepherd, M.U. Gillette, J.A. Lewis and R.G. Nuzzo, *"3D microperiodic hydrogel scaffolds for robust neuronal cultures,"* **21**, 47-54 (2011).

11. J.A. Lewis, *"Direct-write assembly of ceramics from colloidal inks,"* Current Opinion in Solid State and Materials Science, **6**, 245-250 (2002).

12. L. Sun, S.T. Parker, D. Syoji, X. Wang, J.A. Lewis and D.L. Kaplan, *"Direct-write assembly of 3D silk/hydroxyapatite scaffolds for bone co-cultures,"* **1**, 729-735 (2012).

13. D.B. Kolesky, R.L. Truby, A.S. Gladman, T.A. Busbee, K.A. Homan and J.A. Lewis, *"3D bioprinting of vascularized, heterogeneous cell-laden tissue constructs,"* **26**, 3124-3130 (2014).

14. M. Di Biase, P. de Leonardis, V. Castelletto, I.W. Hamley, B. Derby and N. Tirelli, *"Photopolymerization of pluronic F127 diacrylate: A colloid-templated polymerization,"* **7**, 4928 (2011).

15. S. Van Vlierberghe, P. Dubruel and E. Schacht, *"Biopolymer-based hydrogels as scaffolds for tissue engineering applications: A review,"* Biomacromolecules, **12**, 1387-1408 (2011).

16. D. Therriault, S.R. White and J.A. Lewis, *"Rheological behavior of fugitive organic inks for direct-write assembly,"* Applied Rheology, **17**, 10112-11411 (2007).

17. D. Therriault, R.F. Shepherd, S.R. White and J.A. Lewis, *"Fugitive inks for Direct-Write assembly of Three-Dimensional microvascular networks,"* Advanced Materials, **17**, 395-399 (2005).

18. H.G. Muller, *"An introduction to food rheology."* An Introduction to Food Rheology. (1973).

19. C. Rueb and C. Zukoski, *"Viscoelastic properties of colloidal gels,"* Journal of Rheology (1978-Present), **41**, 197-218 (1997).

20. Q. Nguyen and D. Boger, *"Measuring the flow properties of yield stress fluids,"* Annual Review of Fluid Mechanics, **24**, 47-88 (1992).

21. H. Walls, S.B. Caines, A.M. Sanchez and S.A. Khan, *"Yield stress and wall slip phenomena in colloidal silica gels,"* Journal of Rheology (1978-Present), **47**, 847-868 (2003).

22. P. Alexandridis and T. Alan Hatton, *"Poly (ethylene oxide)¸ poly (propylene oxide)¸ poly (ethylene oxide) block copolymer surfactants in aqueous solutions and at interfaces: Thermodynamics, structure, dynamics, and modeling,"* **96**, 1-46 (1995).

23. W. Wu, A. DeConinck and J.A. Lewis, *"Omnidirectional printing of 3D microvascular networks,"* **23**, H178-83 (2011).

24. W. Wu, C.J. Hansen, A.M. Aragon, P.H. Geubelle, S.R. White and J.A. Lewis, *"Direct-write assembly of biomimetic microvascular networks for efficient fluid transport,"* **6**, 739 (2010).

25. K.V. Wong and A. Hernandez, *"A review of additive manufacturing,"* **2012**, 1-10 (2012).

26. X. Liu and P.X. Ma, *"Polymeric scaffolds for bone tissue engineering,"* Annals of Biomedical Engineering, **32**, 477-486 (2004).

27. J.E. Trachtenberg, F.K. Kasper and A.G. Mikos, *"Polymer scaffold fabrication,"* 423-440 (2014).

28. I. Zein, D.W. Hutmacher, K.C. Tan and S.H. Teoh, *"Fused deposition modeling of novel scaffold architectures for tissue engineering applications,"* Biomaterials, **23**, 1169-1185 (2002).

29. S. Kumbar, C. Laurencin and M. Deng, Natural and Synthetic Biomedical Polymers (Newnes. 2014).

30. J.M. Zuidema, C.J. Rivet, R.J. Gilbert and F.A. Morrison, *"A protocol for rheological characterization of hydrogels for tissue engineering strategies,"* Journal of Biomedical Materials Research Part B: Applied Biomaterials, (2013).

31. A.V. Kabanov, E.V. Batrakova and V.Y. Alakhov, *"Pluronic® block copolymers as novel polymer therapeutics for drug and gene delivery,"* Journal of Controlled Release, **82**, 189-212 (2002).

32. D.E. Discher, D.J. Mooney and P.W. Zandstra, *"Growth factors, matrices, and forces combine and control stem cells,"* Science (New York, N.Y.), **324**, 1673-1677 (2009).

33. J.F. Pollock and K.E. Healy, *"Mechanical and swelling characterization of poly (N-isopropyl acrylamide-co-methoxy poly (ethylene glycol) methacrylate) sol–gels,"* Acta Biomaterialia, **6**, 1307-1318 (2010).

34. B. Partee, S.J. Hollister and S. Das, *"Selective laser sintering process optimization for layered manufacturing of CAPA® 6501 polycaprolactone bone tissue engineering scaffolds,"* Journal of Manufacturing Science and Engineering, **128**, 531-540 (2006).

35. D.W. Hutmacher, *"Scaffolds in tissue engineering bone and cartilage,"* Biomaterials, **21**, 2529-2543 (2000).

36. M.N. Collins and C. Birkinshaw, *"Hyaluronic acid based scaffolds for tissue engineering—A review,"* Carbohydrate Polymers, **92**, 1262-1279 (2013).

37. B.K. Mann, A.S. Gobin, A.T. Tsai, R.H. Schmedlen and J.L. West, *"Smooth muscle cell growth in photopolymerized hydrogels with cell adhesive and proteolytically degradable domains: Synthetic ECM analogs for tissue engineering,"* Biomaterials, **22**, 3045-3051 (2001).

38. F. Cellesi, N. Tirelli and J.A. Hubbell, *"Materials for cell encapsulation via a new tandem approach combining reverse thermal gelation and covalent crosslinking,"* Macromolecular Chemistry and Physics, **203**, 1466-1472 (2002).

39. S. Nemir, H.N. Hayenga and J.L. West, *"PEGDA hydrogels with patterned elasticity: Novel tools for the study of cell response to substrate rigidity,"* Biotechnology and Bioengineering, **105**, 636-644 (2010).

40. J. Ramli, A. Hadi, A. Jeefferie and M. Mahat, *"A preliminary study on the effects of photoinitiator and UV curing exposure time to the mechanical and physical properties of the epoxy and vinyl ester fiber glass laminated composites,"* International Journal of Engineering & Technology, **10**(2010).

41. K. Van de Velde and P. Kiekens, *"Biopolymers: Overview of several properties and consequences on their applications,"* Polymer Testing, **21**, 433-442 (2002).